Semiconductor Composites: Strategies for Enhancing Charge Carrier Separation to Improve Photocatalytic Activity

*Roland Marschall**

The formation of semiconductor composites comprising multicomponent or multiphase heterojunctions is a very effective strategy to design highly active photocatalyst systems. This review summarizes the recent strategies to develop such composites, and highlights the most recent developments in the field. After a general introduction into the different strategies to improve photocatalytic activity through formation of heterojunctions, the three different types of heterojunctions are introduced in detail, followed by a historical introduction to semiconductor heterojunction systems and a thorough literature overview. Special chapters describe the highly-investigated carbon nitride heterojunctions as well as very recent developments in terms of multiphase heterojunction formation, including the latest insights into the anatase-rutile system. When carefully designed, semiconductor composites comprising two or three different materials or phases very effectively facilitate charge separation and charge carrier transfer, substantially improving photocatalytic and photoelectrochemical efficiency.

1. Introduction

Converting solar energy into fuels and/or electricity is one of the major scientific challenges researchers are facing nowadays.[1] Mixed oxide semiconductor materials can be used to perform such energy transformation, for example, by converting sunlight energy into chemical energy by catalyzing the formation of chemical bonds. One highly investigated reaction using this approach is photocatalytic water splitting, generating hydrogen and oxygen from water.[2–7] Another example is the photocatalytic reduction of carbon dioxide (CO_2) to carbon-based chemicals.[8]

In case of a semiconductor photocatalyst, the material absorbs sunlight when the energy of the incident photons is equal or larger than the band gap (E_g) of the semiconductor. Thus, an electron is excited from the valence band (VB) of the semiconductor into its conduction band (CB). The photoexcited electron can be used to perform electrochemical reduction reactions on the photocatalyst surface, for example, reducing protons to hydrogen, reducing oxygen to O_2^- radicals, or reducing CO_2, but only if the CB minimum is located at more negative potential than the electrochemical potential of the desired reaction ($H_2/H^+ = -0.41$ V;[2] $CO_2/CH_4 = -0.24$ V;[9] $CO_2/CO_2^- = -1.9$ V;[9] $O_2/O_2^- = -0.33$ V;[10] $.OH,H^+/H_2O = 2.73$ V,[10] all at pH 7). In the VB of the semiconductor, a photo-generated "hole" remains, which can perform electrochemical oxidation of compounds with oxidation potentials more negative than that of the VB maximum. When the photogenerated charge carriers are not used in photocatalytic reactions, they recombine, releasing energy in form of luminescence or heat. The basic principles of these processes are depicted in **Figure 1**.

The basic three steps of photocatalytic reactions are 1) photoexcitation of charge carriers; 2) charge carrier separation and diffusion to the photocatalyst surface; and 3) oxidation and reduction reaction on the catalyst surface. During step (2), recombination can occur via different mechanisms. The major pathway is the already mentioned relaxation of photoexcited electrons back into the VB, which can directly happen from the CB. After the photoexcitation, electrons can also be trapped in electron traps both at and below the surface of a semiconductor, from where the recombination can proceed. The same principle is applicable for the holes, which can also be trapped in interband or surface states. As a result, several possibilities for

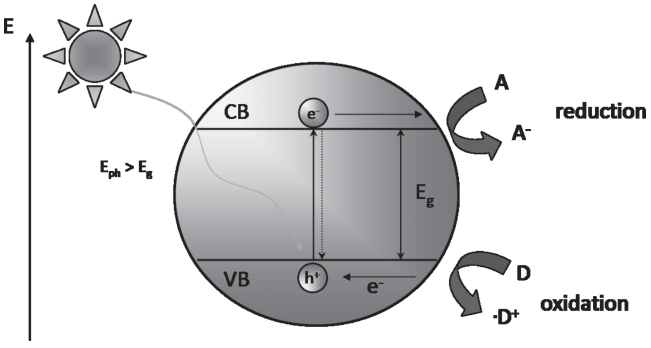

Figure 1. Basic process of charge carrier generation upon light irradiation of a semiconductor particle; E_{ph}: energy of irradiated photon, A: electron acceptor, D: electron donor.

Dr. R. Marschall
Justus-Liebig-University Giessen
Institute of Physical Chemistry
Heinrich-Buff-Ring 58, 35392, Giessen, Germany
E-mail: roland.marschall@phys.chemie.uni-giessen.de

DOI: 10.1002/adfm.201303214

charge carrier recombination exist, summarized in **Figure 2**, which must be inhibited to improve photocatalytic reaction efficiency. [11,12] Those interband or surface states are usually related to defects in the crystal structure or grain boundaries. Therefore, increasing the crystallinity of photocatalyst materials can reduce the recombination probability, as the density of crystal defects is reduced with increasing crystallinity. Moreover, reducing the particle size of a photocatalyst shortens the diffusion pathway of the charge carriers, leading to decreased recombination probability. Finally, charge carrier recombination occurs not only in single particles or on single particle surfaces, but can also occur between different particles.

Several approaches to inhibit charge carrier recombination in heterogeneous photocatalysis are described in the literature. One popular strategy is the decoration of photocatalyst materials with metal nanoparticles: The Fermi energy of the metal nanoparticle is usually lower than that of the semiconductor; facilitating electron transfer from the semiconductor to the metal via the Schottky-contact. The most commonly applied metals for such decoration include platinum (Pt), palladium (Pd), gold (Au), or rhodium (Rh),[13–15] due to their noble and/or catalytic character, but more abundant elements such as cobalt (Co) and nickel (Ni) (both nanoparticles and complexes) have been applied.[16–18] They both act as electron sinks/reservoirs, spatially separating the electrons from the photoexcited holes in the semiconductor VB, and as more efficient active sites for the photocatalytic reduction reaction, thus serving as co-catalysts. Besides metal and also metal oxide (NiO, RuO_2) nanoparticles, other materials like MoS_2, $Rh_{2-y}Cr_yO_3$, or CuO/Cr_2O_3 have been investigated as co-catalysts for, for example, hydrogen generation.[19–21] For catalysis of oxygen generation, classical noble metal oxide co-catalysts such as RuO_2 and IrO_2 are replaced by compounds containing more abundant elements, for example, Mn-oxides, Co-oxides, CoPi, CoBi, and $B_2O_{3-x}N_x$.[22–25] A review summarizing the roles of co-catalysts was published very recently.[26]

Roland Marschall obtained his PhD in Physical Chemistry from the Leibniz University Hannover in 2008. After postdoctoral research at the University of Queensland and the Fraunhofer Institute for Silicate Research ISC, he joined the Industrial Chemistry Laboratory at Ruhr-University Bochum in 2011 as young researcher. Since 07/2013, he is Emmy-Noether Young Investigator at the Justus-Liebig-University Giessen. His current research interest is heterogeneous photocatalysis, especially photocatalytic water splitting using semiconductor mixed oxides.

Another important strategy for the extraction of photoexcited electrons from the semiconductor to reduce charge carrier recombination probability is the formation of composites with carbon materials, especially graphene-based nanoassemblies.[27] Due to the high electron mobility in graphene,[28] photoexcited electrons transferred from the semiconductor CB to graphene are easily separated from the semiconductor surface. Several review articles describe improved photocatalysis achieved with carbon-semiconductor composite nanomaterials.[29–33]

In contrast, the present review will concentrate on the strategy of using two or three different photocatalyst materials

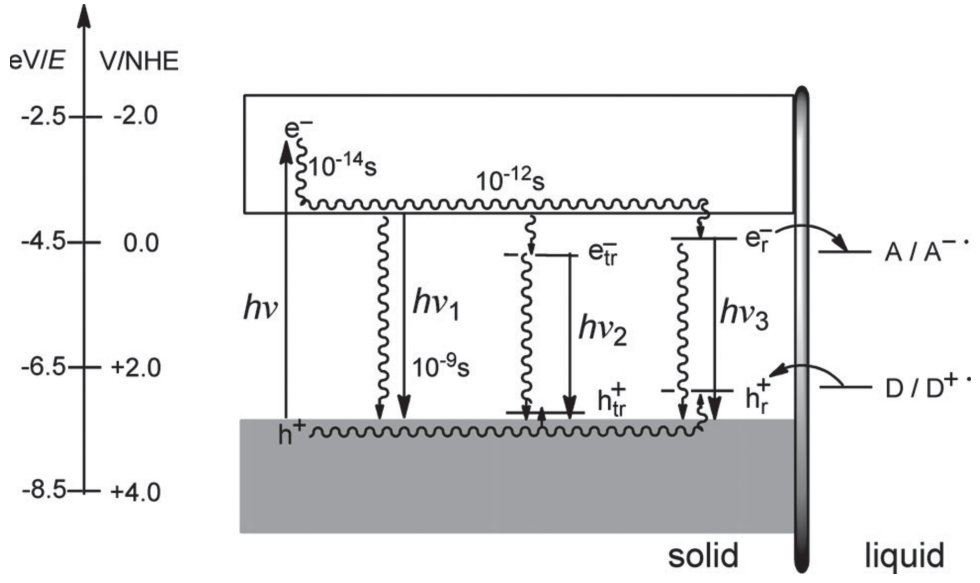

Figure 2. Primary photoprocesses at the semiconductor/liquid interface (thick vertical bar). After photoexcitation, radiative and nonradiative recombination can occur, depicted by straight and waved lines respectively. Electrons and holes gain stability when moving down and up in this scheme, respectively. The depicted band positions apply for TiO_2 in contact with water at pH 7. The electron energy (eV) is given relative to the vacuum level (0 eV); e^-_{tr}: electron trap, h^+_{tr}: hole trap, e^-_r: reactive electron surface site, h^+_r: reactive hole surface site. Reproduced with permission.[12] Copyright 2012, Wiley-VCH.

and/or phases to form heterojunction composites in order to reduce charge carrier recombination. The classical charge transfer between two different photocatalysts will be reviewed, with emphasis on charge carrier transfer and spatial separation of charge carriers on different photocatalysts. However a critical focus of this review comprises the emerging importance of charge carrier separation in multiphase heterojunction materials, which has gained a lot of attention recently, and has not been critically reviewed.

2. Composite Photocatalysts

Although photocatalysis research has made a lot of progress in the last decade, there are still major issues that need to be addressed before photocatalysis can become a viable, efficient and widely accepted process, especially for industrial applications. Practical problems such as long term stability and reliable characterization of photocatalyst performance through standardized reactor geometries and test protocols remain. Additionally, fundamental properties of photocatalyst materials still need improving: critical, fundamental materials design parameters that affect photocatalytic performance include i) electronic structure; ii) surface structure; and iii) crystal structure. In terms of electronic structure, the main tasks for researchers remain both the general improvement of light absorption, and the extension of light absorption of semiconductor materials into the visible portion of the solar spectrum. Several strategies extend the absorption of UV-active photocatalysts into the visible light region, including doping with cations[34–36] and/or anions,[37,38] as well as decoration of the semiconductor with plasmonic metallic nanoparticles.[39–42] One limitation of doping is that it can also reduce the oxidation and reduction potentials of the excited charge carriers, leading to decreased photocatalytic activities. However, alteration of electronic structure via doping can also improve charge carrier mobility in semiconductors, as in the case of, for example, niobium doping of TiO_2.[43,44] Finally, carefully chosen reaction conditions and ideal materials' properties, like doping from the gas phase of a semiconductor material with open crystal structure, can lead to both improved light absorption in the visible light range and enhanced photocatalytic activity.[45–48]

At the level of photocatalyst crystal structure, an ongoing challenge is the reduction of defect concentration to enhance crystallinity, thereby reducing the number of charge carrier recombination sites. The chances of successful bulk diffusion of charge carriers to the reactive photocatalytic interface can also be improved by reducing the particle size and increasing the active surface area of the material. Finally, surface structure and chemistry play important roles in photocatalysis. For example, surface sensitization of UV-active photocatalysts with visible-light absorbing compounds like dyes[49] enables broad spectral absorption for charge carrier generation. Moreover, modification of the photocatalyst surface, particularly with co-catalyst nanoparticles, can lead to improved adsorption of reactants. Finally, tuning the crystal facets of photocatalyst particles like TiO_2, ZnO, WO_3, or α-Fe_2O_3 to expose the most reactive surface facets to the surrounding reactants has attracted considerable attention in the last years.[50–55] Tuning the selectivity of photocatalytic reactions through facet-dependent molecular adsorption becomes possible by fine tuning the ratio of crystal facets.

In summary, the key issues for improving photocatalytic activity are improved light absorption, high crystallinity, large surface area and good charge carrier separation. Optimum band positions, high chemical stability of the semiconductor material, and low cost are also highly desirable. By combining more than one photocatalyst to form a composite photocatalyst system, many of these issues can be addressed at once.

The basic principle for a photocatalyst composite in direct contact will be explained for a system containing two different components. In that case, depending on the band positions of those two semiconductors, the formed heterojunction can be classified into three different types depicted in **Figure 3**. In a type I heterojunction, the VB of semiconductor B is lower than of semiconductor A, and the CB of semiconductor B is higher than the CB of semiconductor A. Since electrons and holes gain energy by moving down and up respectively, photoexcited electrons can transfer from CB(B) to CB(A), while the holes can be transferred from VB(B) to VB(A) when the contact between both materials is sufficient. Thus, all charge carriers are accumulated on semiconductor A, which yields no improvement to charge carrier separation, and thus no improvement in photocatalytic activity. However, this type of heterojunction is quite common, for example, the GaAs–AlGaAs system.[56]

A type II heterojunction provides the optimum band positions for efficient charge carrier separation leading to improved photocatalytic activity. Photoexcited electrons are transferred from CB(B) to CB(A). Whether this occurs directly via electron transfer between semiconductors due to the favorable energetics of the relative positions of the CBs, or due to band bending at the interface inducing an internal electric field is still under debate. Holes are transferred simultaneously from VB(A) to VB(B). Thus, photogenerated electrons and holes are

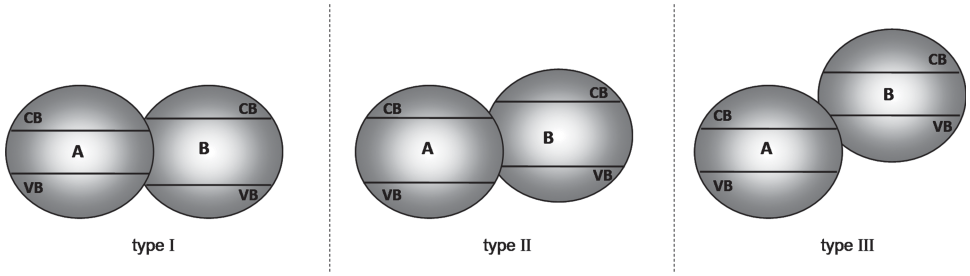

Figure 3. Different types of semiconductor heterojunctions.

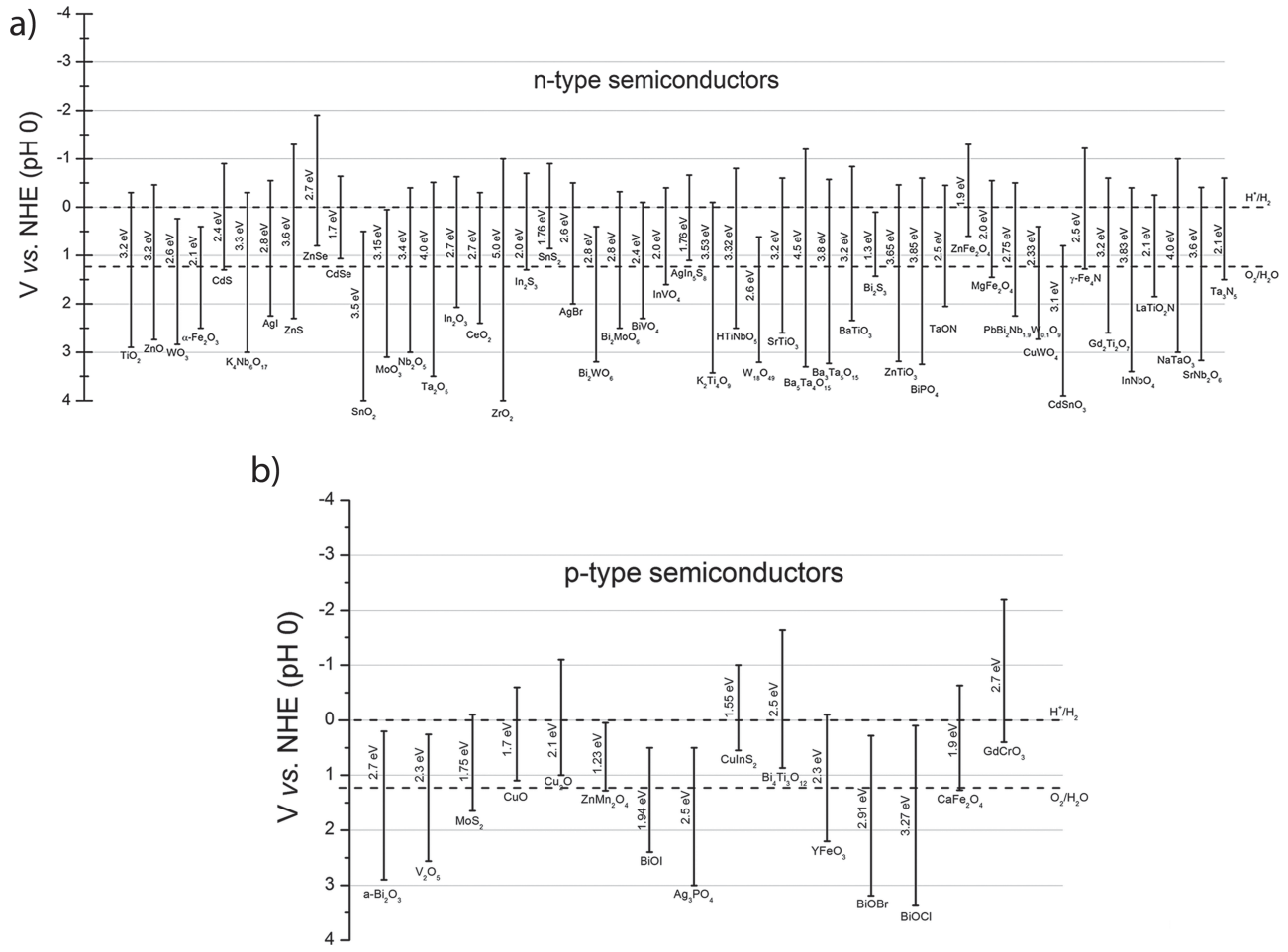

Figure 4. Band gaps and band positions of a) n-type semiconductors and b) p-type semiconductors used for composite photocatalyst heterojunctions. Values taken from references given in the article.

spatially separated from each other, reducing the recombination probability significantly and increasing electron lifetimes, which can be proven by transient spectroscopic techniques. Most of the examples of composite photocatalysts described in the literature are type II heterojunctions.

Finally, in type III heterojunctions the charge carrier transfer is the same as in type II semiconductors, only that the band positions are even further set off. Such arrangements of band positions are also called broken-gap situations.

The following chapters will deal mostly with type II heterostructures. Band positions and band gaps for the presented semiconductors used in heterojunctions are shown in **Figure 4**a,b. In these chapters, the heterojunction-containing materials will be differentiated as follows: A photocatalyst composite consisting of two different materials will be called a "multicomponent" heterojunction material. A composite consisting of different phases of one material (e.g., anatase and rutile, both crystal phases of TiO_2) will be called "multiphase" heterojunction material, since different crystal phases typically also have different band gaps. Sometimes the latter case is also called a homojunction in literature, which would however indicate equal band gaps.

3. Multicomponent Heterojunctions of Semiconductors

3.1. Heterojunctions Between Two/Three Solid State Photocatalysts

One of the first-described and most investigated photocatalyst multicomponent heterojunctions is the CdS/TiO_2 system. Charge transfer of photoexcited electrons from the CB of CdS to TiO_2 was first described in 1984 by Serpone et al.,[57] and further investigated for the CdS–ZnO system by Spanhel et al., in 1987.[58] The charge transfer under visible light irradiation for these heterojunctions is exemplarily shown in **Figure 5**.[59] CdS–ZnO and CdS–TiO_2 are typical examples for type II heterojunctions. Photoexcited electrons are transferred upon light irradiation from the CdS CB to the CB of ZnO or TiO_2. This charge injection process is very fast, it was first reported to occur in <18 ps at CdS–ZnO[59] and <20 ps at CdS–TiO_2, [60] respectively. The charge transfer process is now known to be completed in <2 ps.[61,62] Upon visible light irradiation, only electrons in CdS are excited (E_g = 2.4 eV), while no charge

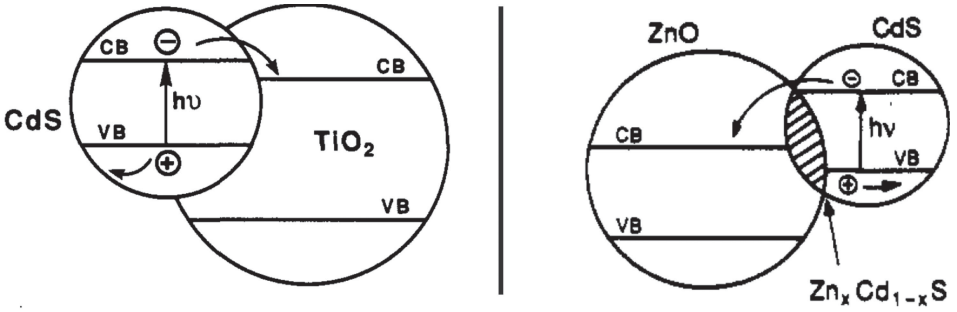

Figure 5. Charge transfer in the CdS/TiO_2 and CdS/ZnO heterojunction composites, band positions are arbitrary and not comparable. Reproduced with permission.[59,60] Copyright 1990/1992, American Chemical Society.

carriers are generated upon visible light irradiation in TiO_2. Therefore, photogenerated holes are only generated in the VB of CdS, and accumulate there due to the higher VB position of CdS with respect to that of TiO_2. The electrons are transferred to TiO_2, and thus spatially separated from CdS reducing the recombination probability. Many early examples of different chalcogenice-containing semiconductor combinations which improve photocatalytic and photoelectrochemical performance have been described, including the above-described CdS–TiO_2,[57,58,60,61,63–65] and CdS–ZnO,[58,59,65,66] but also CdS–$K_4Nb_6O_{17}$,[67] CdS–AgI,[60] Cd_3P_2–TiO_2[68]/ZnO,[69] ZnO–ZnS,[70] ZnO–ZnSe,[71] CdSe–ZnS,[72] and CdS–CdSe.[73] Weller et al. performed a comprehensive study investigating multiple heterostructures (PbS, CdS, Ag_2S, Sb_2S_3, Bi_2S_3 @ TiO_2, Ta_2O_5, Nb_2O_5, ZnO, SnO_2), upon which only heterostructures with CdS and PbS were found to be efficient or stable.[74]

The consequences of such a directed charge carrier transfer under light illumination was nicely shown by Kamat et al. in their investigation of the type II heterojunction between SnO_2 and TiO_2.[75] When both material are in contact, charge carriers are generated in both semiconductors upon UV light irradiation. However, due to their relative band positions (see Figure 4a), charge carriers are separated and the electrons are transferred to the CB of SnO_2. Moreover, all photogenerated holes are accumulated in the VB on TiO_2. When SnO_2 is completely encapsulated by TiO_2, photoexcited electrons cannot react with any reactant and are trapped on SnO_2. This consequence is illustrated in **Figure 6**, in which case photoanodes made of SnO_2–TiO_2 were prepared, and IPCE (incident photon to current efficiency) values were calculated from wavelength dependent photocurrent measurements taken under illumination with UV light. Photoanodes prepared from TiO_2-capped SnO_2 produce hardly any photocurrent, which proves the very effective charge carrier separation. Electrodes made of coupled TiO_2–SnO_2 particles produce anodic photocurrents, as photoexcited electrons are transferred from TiO_2 and SnO_2 to the current-collecting back contact electrode. The improved electron separation was used to decompose the azo dye naphthol blue black (NBB) with electrochemical assistance (up to a degradation rate $k = 0.05$ min^{-1}, 0.8 V vs standard calomel electrode (SCE), 37 ppm NBB in water).[76]

In recent years, the interest especially in CdS–TiO_2 heterojunctions has grown again, due to the emergence of several techniques to prepare CdS quantum dots (QDs) and surface engineered TiO_2 with different morphologies.[77–83] Hoffmann et al. showed that photocatalyst heterojunctions should be carefully designed with regards to the desired application.[81] Using CdS–TiO_2 with deposited Pt co-catalyst, they showed that the deposition of Pt should be exclusively performed on TiO_2 leading to the maximum rate of hydrogen evolution (up to 8.8 mmol h^{-1} per gram catalyst, 25 mL Na_2S/Na_2SO_4 solution [4 mmol L^{-1}], 0.5 g L^{-1}, 450 W Xe lamp, $\lambda > 420$ nm). Charge

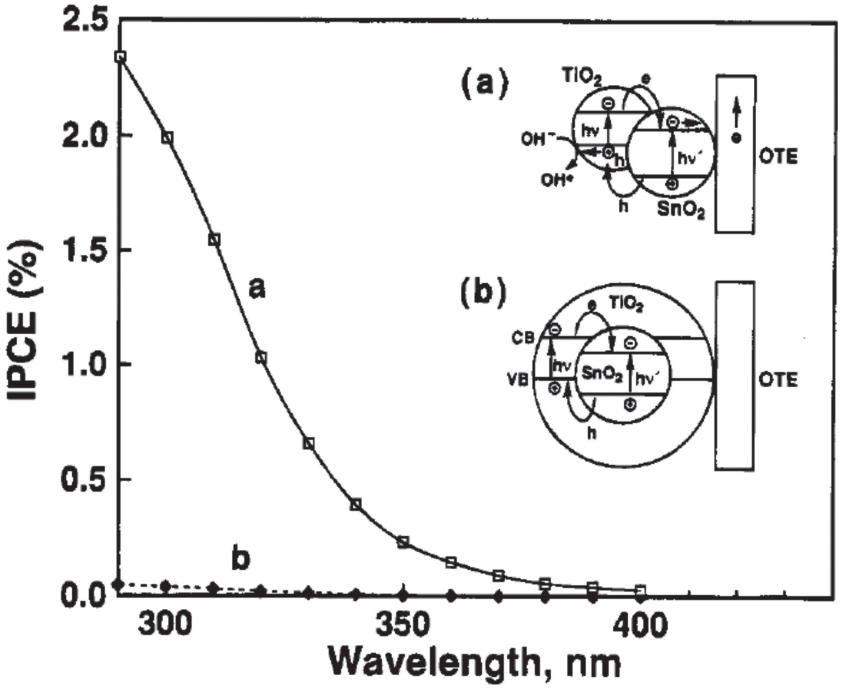

Figure 6. Comparison of IPCE values of a) coupled TiO_2–SnO_2 heterojunction photoanode compared to b) photoanode made of TiO_2-capped SnO_2 particles: OTE: optical transparent electrode. Reproduced with permission.[75] Copyright 1995, American Chemical Society.

separation and vectorial charge transfer of photoexcited electrons from CdS→TiO_2→Pt was achieved, with hydrogen being produced at the surface of the photo-deposited Pt nanoparticles.

Mathur et al. decorated rutile nanorod arrays with CdS QDs to enhance the photocurrent response.[84] To further improve the photoelectrochemical efficiency, a multicomponent-multiphase heterojunction was prepared by introducing an anatase layer onto the rutile nanorods. The resulting "staircase" heterojunction, consisting of a CdS-anatase multicomponent heterojunction and a rutile-anatase multiphase heterojunction, yielded significantly improved photocurrents (up to 2 mA/cm^2 at 0.4 V *vs.* Ag/AgCl, aqueous Na_2S electrolyte, Pt counter, AM 1.5 sun simulator at 1 sun) compared to the single CdS-rutile heterojunction (up to 1 mA cm^{-2} at 0.4 V vs Ag/AgCl).

Besides CdS–TiO_2, many other heterojunction composites have been prepared using TiO_2 to enhance charge carrier separation, as shown in **Table 1**.

The WO_3–TiO_2 system is a typical example for a type I heterojunction: The VB maximum and CB minimum of WO_3 are both energetically situated inside the TiO_2 E_g, so photoexcited charge carriers would be transferred onto WO_3 upon UV light irradiation. However, by selective photodeposition of co-catalysts on one semiconductor of the composite, the photocatalytic properties can nevertheless be tuned to efficiently separate charge carriers even in this type I arrangement.[92]

Diwald et al. used electron paramagnetic resonance spectroscopy (EPR) as an effective technique to detect photogenerated and adsorbed O_2^- ions on ZrO_2–TiO_2 nanoparticle networks.[113] Enhanced charge carrier separation was observed in comparison to pure TiO_2 or pure ZrO_2 nanoparticle networks, due to efficient charge carrier transfer via the ZrO_2–TiO_2 interface, reducing charge carrier recombination in ZrO_2. The same investigations were also performed on TiO_2–SnO_2 nanoparticle networks, proving the electron transfer from TiO_2 to SnO_2 (**Figure 7**) being dependent also on effective mixture and high amount of interfaces between the different nanoparticulate materials.[118]

Heterojunctions can also be used to improve the stability of one component. Ag_3PO_4 usually lacks stability in the absence of sacrificial electron donors, although being highly active in visible light (E_g = 2.5 eV) for photocatalytic reactions. However, forming a heterojunction with TiO_2 significantly improves the stability, and additionally enhances the activity (k = 0.34 min^{-1}, 50 mg catalyst in 100 mL MB [20 mg L^{-1}], 300 W Xe lamp, λ > 400 nm) compared to pure Ag_3PO_4 (k = 0.23 min^{-1} at λ > 400 nm) or TiO_2 (k = 0.14 min^{-1} at λ = 350–800 nm).[148]

Some three-component heterojunctions prepared with TiO_2 have been described, among them are Cu_2O–CuO–TiO_2,[124] CuO–ZnO–TiO_2,[162] TiN–TiO_xN_y–TiO_2,[163] Bi_2O_3/$Bi_4Ti_3O_{12}$/TiO_2,[164] and also heterojunctions containing the multiphase heterojunction rutile-anatase together with SnO_2,[165] WO_3,[166] Cu_2O,[167] and MoO_3.[166] In those cases, charge separation and vectorial charge transfer were achieved over all three components for very effective spatial separation of electrons and holes. More details about the anatase-rutile TiO_2 heterojunctions will be given in Section 4.

More generally, a very large number of different semiconductor combinations have been investigated in terms of their photochemical and photophysical properties. Some of the most prominent and most recent examples are summarized in **Table 2**.

For example, Li et al. prepared hollow spheres of Bi_2WO_6 using polystyrene spheres as template, and a Bi_2O_3 layer was deposited via solvothermal method to prepare a type II composite photocatalyst.[180] This p–n junction between p-type Bi_2O_3 and n-type Bi_2WO_6 lead to strongly improved degradation rates (95% degradation after 3 h, 80 mg catalyst, 80 mL RhB solution [10^{-5} mol L^{-1}], 500 W tungsten–halogen lamp, λ > 420 nm) for RhB compared to pure Bi_2O_3 (2% degradation after 3 h) or Bi_2WO_6 (8% degradation after 3 h).

Marschall et al. prepared a composite of the (111)-layered perovskite $Ba_4Ta_4O_{15}$ and $Ba_3Ta_5O_{15}$ by tuning the ratio of barium and tantalum precursors in their sol–gel syntheses.[174] Although the VB of both phases only differed slightly, the energy difference of both CBs was sufficient to improve charge carrier separation leading to significantly enhanced activity in photocatalytic TA hydroxylation and H_2 generation from aqueous methanol (1885 µmol h^{-1} per 0.5 g catalyst, in 600 ml methanol/H_2O [8 vol%], 350 W Hg immersion lamp, compared to 800 µmol h^{-1} per 0.5 g pure $Ba_4Ta_4O_{15}$), with very low amounts (0.025 wt%) Rh co-catalyst.

Chai et al. prepared a photocatalyst composite made of BiOCl and Bi_2O_3 in 2009 which was very active for 2-propanol oxidation (k = 0.602 h^{-1} m^{-2}, 117 ppmv 2-propanol, 300 W Xe lamp, λ > 420 nm).[184] However, the mechanism responsible for visible light activity was different from those deriving from more typical sensitization strategies. Under visible light irradiation, photogenerated charge carriers can only be produced on Bi_2O_3, but since its VB is 0.7 eV lower than that of BiOCl, electrons from the VB of BiOCl can be transferred to the VB hole in Bi_2O_3, resulting in reactive holes in the BiOCl VB which can oxidize of organic compounds. Thus, electrons and holes become spatially separated, decreasing recombination probability and resulting in increased reaction rates.

Madhusudan et al. combined $BiVO_4$ with photocatalyst $Bi_2O_2CO_3$.[187] SEM images revealed a nanocomposite of $Bi_2O_2CO_3$ nanosheets with highly exposed {001} facets combined with $BiVO_4$ particles which were prepared by a hydrothermal process. The resulting type II heterojunction was both stable and very effective for RhB degradation in visible light (97% degradation in 60 min, 0.1 g catalyst in 20 mL RhB solution [2 x 10^{-5} mol L^{-1}], 350 W Xe Lamp, λ > 420 nm) compared to the single components ($BiVO_4$: 54% in 60 min, $Bi_2O_2CO_3$: 47% in 60 min). Saito et al. used $BiVO_4$ in a triple multicomponent heterojunction together with SnO_2 and WO_3 to create a very effective vectorial charge transfer system for photoexcited electrons.[189] First, WO_3 was deposited on FTO (fluorine-doped tin oxide) electrode via spin-coating, followed by spin coating of SnO_2 and $BiVO_4$ subsequently. The resulting multilayer photoanode was irradiated with visible light from the $BiVO_4$ side, upon which charge carriers were mainly generated in the $BiVO_4$ layer, but also in WO_3. In addition to having VB and CB bands well-positioned for electron transfer, the SnO_2 interlayer also interposed an energy barrier to the recombination process between electrons in the CB of WO_3 and the holes in the VB of $BiVO_4$, improving the overall photoelectrochemical performance in $KHCO_3$ electrolyte. Stoichiometric photoelectrochemical water splitting was achieved using a Pt counter electrode (0.1 M $KHCO_3$ electrolyte) with

Table 1. Prominent multicomponent heterojunctions with TiO_2.

Semiconductor 1	Semiconductor 2	Type of heterojunction	Photocatalysis in visible light ($\lambda > 400$ nm)	Refs.
TiO_2	ZnO	II	-	[85,86]
	WO_3	I	Isopropyl alcohol (IPA) oxidation, stearic acid removal, Rhodamine B (RhB) degradation, oxalic acid oxidation, H_2 production, formic acid oxidation, enhanced photocurrents	[87–96]
	MoS_2	I	enhanced photocurrents, H_2 production, RhB degradation	[97,98]
	MoO_3	II	–	[87,99,100]
	Nb_2O_5	I	–	[101,102]
	Bi_2O_3	II	Orange II oxidation, p-chlorophenol degradation, pentachlorophenol degradation	[103]
	In_2O_3	II	2-chlorophenol degradation, 2,4-dichlorophenoxyacetic acid oxidation, RhB degradation	[106–109]
	CeO_2	I/II	Iodide oxidation, Methylene blue (MB) degradation, Methyl Orange (MO) degradation	[110–112]
	ZrO_2	I	–	[113,114]
	V_2O_5	I/II	RhB degradation, terephthalic acid (TA) hydroxylation, H_2 production	[115–117]
	SnO_2	II	–	[118]
	Fe_2O_3	I	enhanced photocurrents, H_2 production, RhB degradation	[119–122]
	CuO	II	H_2 production, Orange II oxidation	[123,124]
	Cu_2O	II	Orange II oxidation, MB degradation, p-nitrophenol oxidation, 2,4,6-trichlorophenol degradation, enhanced photocurrents	[103,125–127]
	In_2S_3	II	MO degradation, H_2 production	[128–130]
	SnS_2	II	Cr(VI) reduction, 4-chlorophenol (4-CP) degradation, phenol degradation, MO degradation, RhB degradation	[131]
	BiOI	I	MO degradation,	[132,133]
	$ZnIn_2S_4$		enhanced photocurrents	[134]
	Ag-AgBr	II	Phenol degradation, ibuprofen degradation, *E. coli* treatment, enhanced photocurrents	[135–137]
	Bi_2WO_6	II	RhB degradation, acetaldehyde oxidation, stearic acid removal, enhanced photocurrents	[138–142]
	Bi_2MoO_6	II	RhB degradation, alizarin red degradation	[143,144]
	$InVO_4$	II	benzene oxidation, cyclohexane oxidation, ethylbenzene oxidation, toluene oxidation, acetone oxidation, *E. coli* treatment	[145,146]
	$BiVO_4$	I	benzene oxidation	[147]
	Ag_3PO_4	II	RhB degradation, MB degradation, 2-CP degradation, enhanced photocurrents	[148,149]
	$Bi_{12}TiO_{20}$	II	RhB degradation	[150]
	$AgIn_5S_8$	II	H_2 production	[151]
	$CuInS_2$	II	4-nitrophenol degradation	[152]
	$AgGaS_2$		H_2 production	[153]
	$CoFe_2O_4$	II	enhanced photocurrents	[154]
	$ZnMn_2O_4$	I	Orange II oxidation	[103]
	$K_2Ti_4O_9$	I	–	[155,156]
	$HTiNbO_5$	II	–	[157]
	$Bi_4Ti_3O_{12}$	II	RhB degradation	[158]
	$W_{18}O_{49}$	II	IPA oxidation	[159]
	$YFeO_3$	II	benzene oxidation, Orange II oxidation	[160,161]

IPCE values above 40% >400 nm. The photoelectrochemical performance of $BiVO_4$ was enhanced by Jeong et al. via Mo and W doping.[191] Additionally, they electrochemically deposited the well-known oxygen evolution co-catalyst Co-Pi[23] on their resulting WO_3-$BiVO_4$:Mo heterojunction photoanode, reducing bulk and surface recombination significantly, and improving charge injection and charge separation. Photocurrents up to 2.4 mA cm^{-2} at 1.23 V versus RHE were achieved.

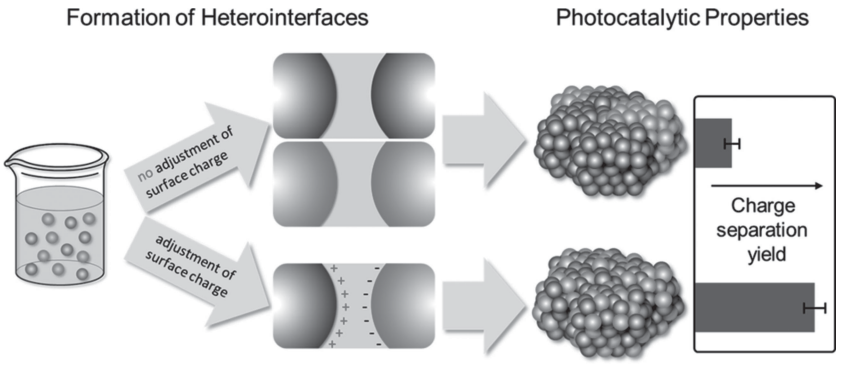

Figure 7. Synthesis of TiO_2–SnO_2 nanoparticle network, homogeneous distribution achieved by adjustment of surface charges leading to increased number of interfaces and enhanced charge separation yield. Reproduced with permission.[118] Copyright 2012, American Chemical Society.

Kim et al. prepared a composite photoanode by coating an overlayer of p-type $CaFe_2O_4$ particles onto n-type TaON.[196] Resulting photocurrents were strongly enhanced by combination of these two semiconductors compared to those observed at single TaON electrodes, IPCE values increased from 5% to 30% at 400 nm (in 0.5 mol L^{-1} NaOH at 0.2 V vs Ag/AgCl). Stoichiometric photoelectrochemical water slitting was achieved with a Faradaic efficiency of ≈80% from potassium phosphate buffered KOH solution at pH 11 with Pt counter electrode and a 0.4 V applied bias versus Ag/AgCl at $l > 420$ nm.

Table 2. Multicomponent heterojunctions for enhanced charge carrier separation.

Semiconductor 1	Semiconductor 2	Semiconductor 3	Type of heterojunction	Photocatalysis in visible light (λ > 400 nm)	Refs.
Ag_2O	Bi_2WO_6		II	MO degradation	[168]
Ag_2O	Bi_2O_3		II	MO degradation	[169]
Ag_3PO_4	Cr:$SrTiO_3$		II	IPA oxidation	[170]
AgBr	BiOBr		II	RhB degradation	[171]
Ag/AgCl	$BiMg_2VO_6$		II	Acid red G (ARG) degradation	[172]
AgI	SnO_2		II	MB degradation	[173]
$Ba_5Ta_4O_{15}$	$Ba_3Ta_5O_{15}$			H_2 generation, TA hydroxylation	[174]
$Bi_2O_2CO_3$	Bi_2MoO_6	Carbon nitride	II	RhB degradation	[175]
Bi_2O_3	$BaTiO_3$		II	RhB/MO degradation	[176,177]
β-Bi_2O_3	Bi_2MoO_6		II	RhB degradation, *E.coli* destruction	[178]
Bi_2O_3	ZnO		I/II	–	[179]
Bi_2O_3	Bi_2WO_6		II	RhB degradation	[180]
Bi_2S_3	BiOCl		II	2,4-dichlorophenol degradation	[181]
Bi_2S_3	Bi_2WO_6		II	Phenol degradation	[182]
BiOBr	Bi_2WO_6		II	RhB degradation MO degradation	[183]
BiOCl	Bi_2O_3		II	IPA oxidation, TA hydroxylation	[184]
BiOI	$ZnTiO_3$		II	Rhodamine 6G (R6G) degradation	[185]
$BiPO_4$	$BiVO_4$		II	MB degradation	[186]
$BiVO_4$	$Bi_2O_2CO_3$		II	RhB degradation	[187]
$BiVO_4$	$CuWO_4$		II	enhanced photocurrents	[188]
$BiVO_4$	SnO_2	WO_3	II-I	enhanced photocurrents	[189]
$BiVO_4$	FeOOH		-	enhanced photocurrents, O_2 evolution	[190]
$BiVO_4$	WO_3		II	enhanced photocurrents	[191]
$BiVO_4$	Cu_2O		II	MB degradation, Phenol degradation	[192]
$BiVO_4$	CuO		II	MB degradation	[193]
$BiVO_4$	V_2O_5		II	MB degradation	[194]
$CaAl_2O_4$:(Eu,Nd)	(Ta,N)-TiO_2	Fe_2O_3	II	Acetaldehyde oxidation	[195]
$CaFe_2O_4$	TaON		II	Enhanced photocurrents, H_2O splitting	[196]
$CaFe_2O_4$	$ZnFe_2O_4$		II	Enhanced photocurrents	[197]
$CaFe_2O_4$	$MgFe_2O_4$		II	IPA oxidation, H_2 generation	[198]
$CaFe_2O_4$	$PbBi_2Nb_{1.9}W_{0.1}O_9$		II	H_2 evolution, O_2 evolution, IPA oxidation, acetaldehyde oxidation	[199]
$CaFe_2O_4$	WO_3		II	Acetaldehyde oxidation	[200]
CdS	$KNbO_3$		II	H_2 generation	[201]
CdS	$CdSnO_3$		II	RhB degradation	[202]
CdS	NiO		II	H_2 generation	[203]

Table 2. Continued.

Semiconductor 1	Semiconductor 2	Semiconductor 3	Type of heterojunction	Photocatalysis in visible light (λ > 400 nm)	Refs.
CdS	SnO_2	Ru-complex	II	Enhanced photoconversion efficiency	[204]
CdS	ZnO		II	H_2 generation	[205,206]
CdS	Al_2O_3		II	H_2 generation	[205]
CdS	CdSe		I	H_2 generation	[207]
CdS	ZnS		I	H_2 generation	[208]
CdS	ZnS	CdTe		H_2 generation	[208]
CdS	MoS_2		II	H_2 generation, enhanced photocurrents	[19,209]
CdS	Ta_2O_5		II	H_2 generation with simultaneous pollutant degradation	[210]
CdS	$ZnFe_2O_4$		II	H_2 generation	[211]
CdSe	MoS_2		II	H_2 generation	[212]
Cu_2O	CuO		II	enhanced photocurrents	[213]
CuO	In_2O_3		II	RhB degradation	[214]
CuS	ZnS			H_2 generation	[215]
Fe_2O_3	$SrTiO_3$		I	Ag^+ reduction	[216,217]
Fe_2O_3	graphene	$BiVMoO_4$	II	enhanced photocurrents	[218]
Co:Fe_2O_3	$MgFe_2O_4$		II	enhanced photocurrents	[219]
Ti:Fe_2O_3	$ZnFe_2O_4$		II	enhanced photocurrents	[220]
Fe_2O_3	$ZnFe_2O_4$		II	enhanced photocurrents	[221]
Fe_2O_3	Fe_4N		II	H_2O splitting	[222]
Fe_3O_4	SiO_2	Bi_2WO_6	–	RhB degradation	[223]
Fe_3O_4	SiO_2	Au-TiO_2	–	MB degradation	[224]
$Gd_2Ti_2O_7$	$GdCrO_3$		II	H_2 generation	[225]
Cr:In_2O_3	Cr:$Ba_2In_2O_5$		II	H_2 generation, O_2 generation, H_2O splitting	[226]
In_2O_3	$Gd_2Ti_2O_7$		II	H_2 generation, enhanced photocurrents	[227]
In_2O_3	N:$InNbO_4$		II	H_2 generation	[228]
In_2O_3	$LaTiO_2N$		II	enhanced photocurrents	[229]
$NaTaO_3$	$SrTiO_3$		I	–	[230]
Nb_2O_5	$SrNb_2O_6$		II	–	[231]
SnO_2	V_2O_5		II	–	[232]
$SrTiO_3$	TiO_2		II	–	[233]
Sr_2TiO_4:(La,Cr)	$SrTiO_3$:(La,Cr)		II	H_2 generation, enhanced photocurrents	[234]
Ta_3N_5	TaON		II	O_2 evolution, MB degradation, enhanced photocurrents	[235]
$H_{0.68}Ti_{1.83}O_4$-nanosheets	Zn-Cr-LDH nanosheets		II	O_2 generation	[236]
CdS	MIL-101		-	H_2 generation	[237]
WO_3	Sb_2O_3		II	RhB degradation	[238]
WO_3	Si		II	enhanced photocurrents	[239]
WO_3	Bi_2WO_6		II	H_2O splitting, enhanced photocurrents	[240]
WO_3	H_2WO_4		II	RhB degradation	[241]
WO_3	Fe_2O_3		II	enhanced photocurrents	[242]
WO_3	$BiVO_4$		II	enhanced photocurrents	[243]
$_yBiO(Cl_xBr_{1-x})$	Bismuth oxide hydrate		II	RhB degradation, KI oxidation, Acetophenone degradation	[244]
ZnO	$Cs_{0.68}Ti_{1.83}O_4$		I	–	[245]
ZnO	Au/$ZnFe_2O_4$		II	enhanced photocurrents	[246]
ZnO	$Ti_{1.83-x}Fe_xO_4$ nanosheets		II	MB degradation	[247]
ZnO	BiOI		II	MO degradation, enhanced photocurrents	[248]
ZnO	Fe_2O_3		II	H_2 generation, R6G degradation, 4-chloro-2-nitro phenol degradation	[249]
ZnO	In_2O_3		II	MB degradation	[250]
ZnO	CdS	Cd	II	H_2 generation	[251]
ZnO	ZnSe		II	Orange-II degradation	[252]
ZnS	$[Fe_2S_2]$		I	H_2 generation	[253]

In 2008, Zong et al. investigated different co-catalyst loadings on CdS, and discovered that MoS_2 was very effective as H_2 generation co-catalyst due to the ideal junction between those two compounds (up to 500 μmol h^{-1} per 0.1 g catalyst, 200 mL lactic solution [10 vol%], 300 W Xe lamp, $l > 420$ nm).[19] Liu et al. further investigated the MoS_2–CdS system and identified MoS_2 as a p-type semiconductor from Mott-Schottky-plots, with holes as major charge carriers but having low carrier density.[209] In a MoS_2-CdS p-n-heterojunction in the form of a double-layer electrode comprising electrodeposited CdS coated with MoS_2 deposited from bath deposition, the photocorrosion of CdS was inhibited and charge carrier separation improved, leading to significantly enhanced IPCE values under UV and visible light irradiation (from 4% of pure CdS up to 30% at 400 nm for the composite electrode, collected at 0 V vs Ag/AgCl). Seger et al. electrodeposited MoS_x onto a p-type Si electrode with high level of surface n-doping (n^+p-Si).[254] To enhance the stability against oxidation during H_2 generation, a thin Ti-TiO_x layer was introduced, resulting in the heterojunction composite photocathode shown in **Figure 8**. H_2 was generated under chronoamperometric testing (200 μmol/h/cm^2) using only the red part ($l > 635$ nm) of the solar spectrum (AM1.5) wasAM1.5), shown in $HClO_4$ electrolyte with an H_2-purged Pt counter electrode.

Hematite (α-Fe_2O_3) has been used extensively to construct composite photoanodes (see table 2). For example, hematite was combined with zinc ferrite $ZnFe_2O_4$ to prepare nanoparticulate heterojunction photoanodes.[221] The increased current density (from 0.02 to 0.06 mA cm^{-2} at 0.4 V vs Ag/AgCl, 1 M NaOH, 300 W Xe lamp, AM 1.5 filter, 1 sun) was proven to originate mainly from enhanced electron-hole separation in the type II heterojunction, introducing Al^{3+} and Co^{2+} ions to the electrode surface further improved the overall photocurrent up to 0.45 mA cm^{-2} at 0.4 V versus Ag/AgCl. Recently, Hou et al. used Co-doped hematite nanorods grown on a Ti mesh as substrate for deposition of $MgFe_2O_4$, constructing a flexible type II heterojunction photoanode absorbing a wide range of visible light, and based only on earth-abundant elements.[219] The complex structure of the photoanode (**Figure 9**) with large contact area enabled enhanced photocurrents (in 0.01 mol/L NaOH, vs Ag/AgCl) under sunlight (150 W Xe lamp, AM 1.5G filter) irradiation and photoelectrochemical O_2 gas evolution (≈5.7 L m^{-2} per hour, 0.5 V applied bias, 0.01 M NaSO4 electrolyte, Pt counter electrode evolving stoichiometric H_2, Ag/AgCl reference) with a Faradaic efficiency of ≈98%.

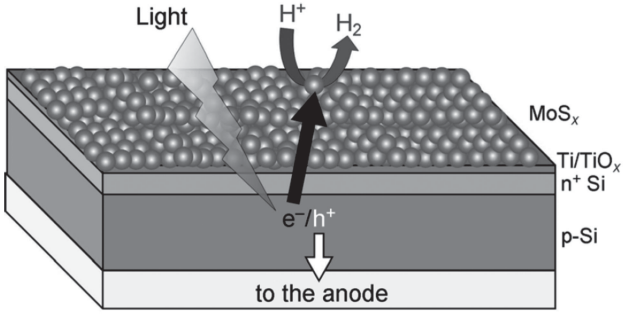

Figure 8. Scheme of the MoS*x*–Ti-n^+p-Si photocathode prepared by Seger et al. Reproduced with permission.[254] Copyright 2012, Wiley-VCH.

Jia et al. prepared a type II heterojunction of two (La,Cr)-doped strontium titanates, $SrTiO_3$ and Sr_2TiO_4.[234] Both titanates are able to absorb visible light only after (La,Cr)-doping, and are n-type semiconductors according to Mott-Schottky-measurements. Thus, both are able to generate H_2 from aqueous methanol solutions under visible light irradiation with Pt co-catalyst (La,Cr-doped $SrTiO_3$: 2 μmol/h per 0.5 g; La,Cr-doped Sr_2TiO_4: 2 μmol h^{-1} per 0.5 g, 200 mL methanol/H_2O [20 vol%], 300 W Xe lamp, $l > 420$ nm, no co-catalyst). (La,Cr)-doped Sr_2TiO_4 has lower CB and VB positions. After combination of both doped semiconductors, electrons excited by visible light irradiation of the heterojunction are transferred and accumulated in the CB of (La,Cr)-doped Sr_2TiO_4, while the holes are accumulating in the VB of (La,Cr)-doped $SrTiO_3$. Forming this heterostructure, improved H_2 generation rates were observed (12 μmol h^{-1} per 0.5 g catalyst). Preferential Pt loading on the surface of (La,Cr)-doped Sr_2TiO_4 (the electron-accepting component in the heterojunction) lead to further enhanced H_2 evolution rates (16 μmol h^{-1} per 0.5 g catalyst, 0.25 wt% Pt) and more long-lived electrons due to efficient charge carrier separation measured by time resolved FT-IR spectroscopy.

Gunjakar et al. combined titanate nanosheets (prepared from proton-exchanged and delaminated layered titanate $Cs_{0.68}Ti_{1.83}O_4$) and delaminated nanosheets prepared from Zn–Cr-layered-double hydroxide (Zn–Cr-LDH) to design mesoporous heterolayered nanocomposites.[236] Layered titanate nanosheets exhibit a negative surface charge, while the delaminated LDH nanosheets are positively charged. Thus, both nanosheets can be alternately restacked. Depending on the ratio of the nanosheets, a house-of-cards like mesoporosity was generated, and the photocatalytic O_2 evolution (10 mg catalyst in 20 mL $AgNO_3$ [0.01 mol L^{-1}], 450 W Xe lamp, $l > 420$ nm) was enhanced (from 6.7 μmol h^{-1} per 0.01 g catalyst for Zn–Cr-LDH to 11.8 μmol h^{-1} per 0.01 g catalyst) forming these heterostructures. Since the photocatalytic activity was achieved in visible light, the LDH must absorb the photons provided by the Xe lamp. Electrons are then transferred to the CB of the titanate for charge separation. Additionally, by covering the Zn–Cr-LDH nanosheets with titanate nanosheets, the stability of the LDH nanosheets regarding Zn dissolution was significantly improved. The same layered titanate nanosheets were also used to prepare heterojunctions with ZnO for improved pollutant (Phenol, DCA) degradation (400 W Xe lamp, $l > 300$ nm).[245]

Wang et al. prepared CdS@Cd core–shell particles decorated with ZnO nanoparticles for improved H_2 generation.[251] In this case, the Cd metal core provided the channel for fast charge carrier transport: Upon light irradiation, charge carriers are excited either in CdS and ZnO. H_2 evolution occurs at the CdS surface, the oxidation reaction at ZnO. Thus, the remaining charge carriers (holes on CdS, electrons on ZnO) recombine via Cd metal contact, leaving no charge carriers on CdS or ZnO behind (Z-scheme type mechanism), leading to photocatalytic activity for H_2 evolution on the CdS surface of up to 610 μmol h^{-1} per 0.1 g catalyst (300 mL solution of Na_2S [0.1 mol L^{-1}] and Na_2SO_3 [0.1 mol L^{-1}], 300 W Xe lamp),

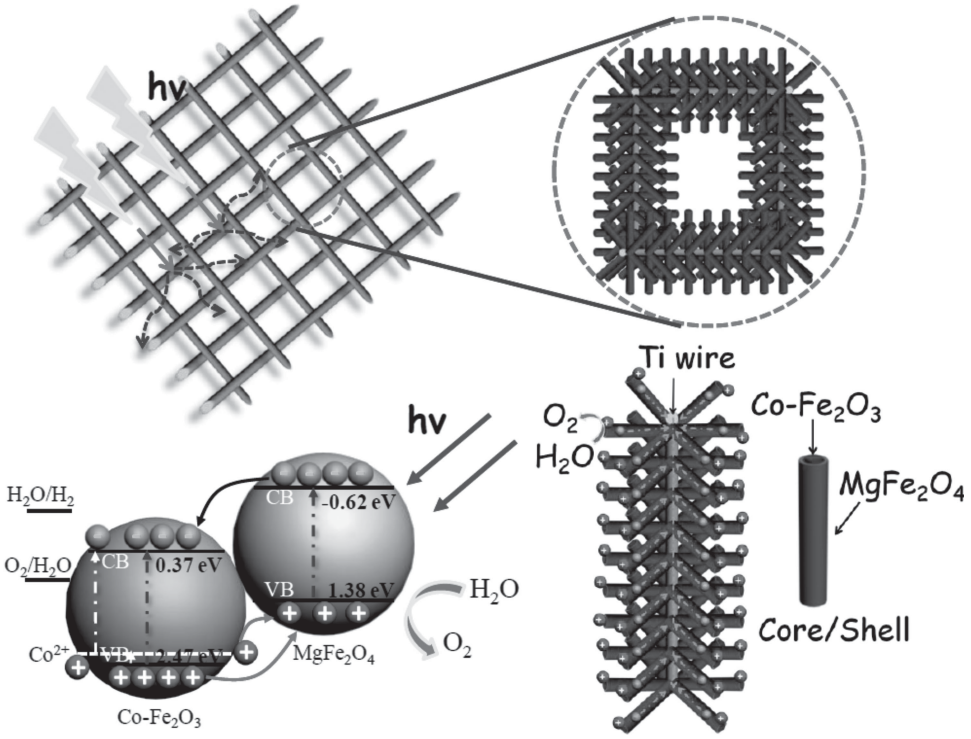

Figure 9. Scheme of a photocathode made of $MgFe_2O_4$-covered, Co-doped hematite nanorods grown on a Ti-mesh, and respective band positions for charge separation. Reproduced with permission.[219] Copyright 2013, Wiley-VCH.

≈50× higher than for pure CdS (12 μmol h^{-1} per 0.1 g catalyst). Loading the ZnO–CdS@Cd composites with 3 wt% Pt further improved the activity to a maximum of 1920 μmol h^{-1} per 0.1 g catalyst, one of the highest reported hydrogen evolution rates for composite photocatalysts.

3.2. Metal Oxide–Carbon Nitride Heterojunctions

Carbon-nitrogen based polymers belong to the oldest reported polymer materials prepared by chemists. Berzelius in 1830 and Justus Liebig in 1834 reported a yellowish compound consisting only of carbon and nitrogen, which Liebig received after decomposition of $(CN)_2S$ and called "Melon".[255] In 2006, Mitoraj and Kisch determined that the origin of visible light activity of TiO_2 after treatment/modification with urea was related to surface sensitization with higher melamine condensation products[256] like "Melon". Urea was converted to ammonia and isocyanic acid between 300–420 °C in the presence of TiO_2, and the resulting melamine was further condensed to "Melon" on the surface of TiO_2. Since Antonietti et al. described the optical properties, the electronic structure and the photocatalytic activity of layered carbon nitride photocatalysts in detail in 2009,[257] the material has been investigated by many research groups all over the world in diverse attempts to optimize its optical, electronic and catalytic properties.[258] One of the very interesting and important features of carbon nitride is its relatively low E_g (2.7 eV) and its high VB and CB positions (+1.4 V and –1.3 V at pH 7 *vs.* normal hydrogen electrode (NHE), respectively) compared to those of many oxide semiconductors.[259] Therefore, many different type II heterojunction composites with oxide semiconductors have been reported using carbon nitride. Several groups have recently investigated the properties of carbon nitride-TiO_2 composites.[260–265] Bledowski et al. showed that the in-situ formation of carbon nitride (here called polyheptazine) in the presence of TiO_2 leads to very intensive interfacial contact between both semiconductors, resulting in a core–shell morphology.[262] Besides the expected photoinduced charge transfer of photoexcited electrons from the CB of carbon nitride to the CB of TiO_2, indications for a direct optical excitation from the VB of carbon nitride to the CB of TiO_2 were found, and attributed to the aforementioned optimized interfacial contact. Stable photocurrents were measured under continuous visible light (λ > 455 nm) irradiation supporting this assumption. However, oxygen evolution experiments, after deposition of IrO_2 nanoparticles as co-catalysts, were only conducted at λ > 420 nm, which do not rule out the typically observed excitation process (from carbon nitride VB to carbon nitride CB) followed by photoinduced charge transfer of photoexcited electrons from the carbon nitride CB to the TiO_2 CB for the overall photocatalytic process.

Carbon nitride has also been used to prepare composite photocatalyst systems with Ag_3PO_4,[266] Bi_2WO_6,[267,268] $Bi_5Nb_3O_{15}$,[269] BiOBr,[270,271] CdS,[272,273] $CuInS_2$,[274] Fe_2O_3,[275] Fe_3O_4,[276] N-$H_2Ta_2O_6$,[277] MoS_2,[278] N-Nb_2O_5,[279] $SrTiO_3$,[280,281] TaON,[282] WO_3,[283] ZnO,[284] and $ZnWO_4$[285] with enhanced catalytic activity due to improved charge carrier separation relative to that of non-composite materials. Pan et al. covered $BiPO_4$ nanorods with carbon nitride to achieve a composite

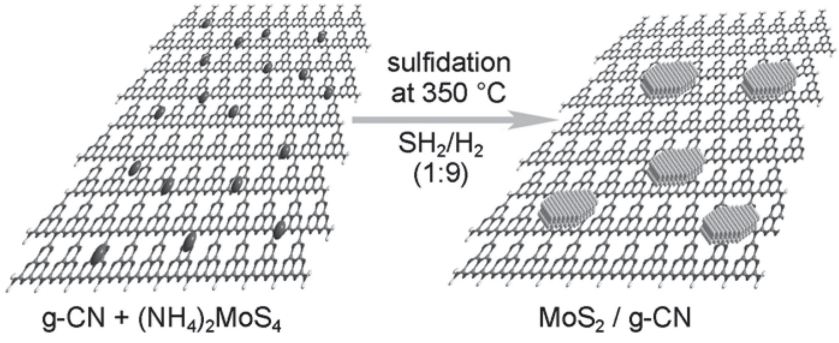

Figure 10. Preparation of MoS_2-decorated carbon nitride (g-CN) forming a p-n-multicomponent type II heterojunction. Reproduced with permission.[287] Copyright 2013, Wiley-VCH.

photocatalyst with core–shell structure,[286] leading to enhanced photocatalytic activity in visible light for MB degradation, up to $k = 0.3$ h^{-1} for the composite compared to $k = 0.05$ h^{-1} for the carbon nitride (50 mg catalyst in 100 mL MB [10^{-5} mol L^{-1}], 500 W Xe lamp, $\lambda > 420$ nm). Huo et al. prepared a 2D layered type I heterojunction composite of carbon nitride with layered MoS_2 to enhance photocatalytic H_2 generation.[287] The morphological similarity between both sheet-like compounds (**Figure 10**) facilitated the planar growth of MoS_2: the intimate contact between both materials was shown to be important for enhanced photocatalytic activity of the composite. Additionally, low amounts (0.2 wt%) of MoS_2 were necessary to optimize H_2 generation rates in the presence of lactic acid (100 mL solution [10 vol%]) as an electron donor (up to 27 μmol h^{-1} per 0.02 g catalyst, 300 W Xe lamp, $\lambda > 420$ nm, apparent quantum yield (AQY, number of evolved $H_2 \times 2$ divided by number of incident photons): 2.1% at 420 nm).

Yuan et al. used the elemental photocatalyst red phosphor[288] to construct a metal free composite with carbon nitride.[289] The composite showed strongly enhanced visible light absorption compared to pure carbon nitride, and at 30 wt.-% of carbon nitride, the maximum rates for photocatalytic H_2 generation (up to 10 μmol h^{-1} per 0.01 g catalyst, in 10 mL aqueous L-ascorbic acid [0.1 mol L^{-1}], 0.5 wt% Pt, 300 W Xe lamp, $\lambda > 420$ nm) or CO_2 reduction (20 mg catalyst, 0.5 wt% Pt, 500 W Xe lamp) were achieved. Another metal free semiconductor multicomponent type II heterojunction was prepared by Zhang et al., using sulphur-modified carbon nitride in combination with conventional carbon nitride.[290] The resulting composite showed longer charge carrier lifetimes, enhanced H_2 generation activities (up to 130 μmol h^{-1} per 0.02 g catalyst, in 100 mL aqueous triethanolamine [10 vol%], 300 W Xe lamp, $\lambda > 420$ nm) and improved photocurrent densities.

4. Multiphase Heterojunctions of Semiconductor Photocatalysts

Since the electronic structure of a semiconductor depends on the atomic ordering hence the crystal structure, different crystal phases of one semiconductor compound can exhibit different band positions and/or E_g. Thus, composites of multiple crystal phases can be prepared to achieve enhanced charge carrier separation when the band positions are suitable to each other. The resulting multiphase heterojunctions can be of type I–III.

The most prominent example for a photocatalyst compound with different active phases is TiO_2 with anatase, rutile or brookite crystal structures. All three crystal structures exhibit different photocatalytic properties, with anatase usually considered the most active due to better organic molecule adsorption[291] and lower recombination rate.[292] However, there are also reports showing higher activity for rutile or brookite, described later in this chapter.

All three kinds of double-phase heterojunctions of the different TiO_2 phase have been reported in literature. Evonik-Degussa Aeroxide TiO_2 P25 (in the following denoted as P25), an anatase–rutile heterojunction with ~80:20 phase composition (varies with different reports) is often considered as benchmark material for photocatalytic reactions, and its high activity is often attributed to the synergy between anatase and rutile. This effect was first proposed by Bickley et al. in 1991.[293] Evidence for the proposed synergy of anatase and rutile in P25 was found by Ohno et al., investigating the photocatalytic naphthalene oxidation on pure anatase, pure rutile and P25.[294,295] The reaction was found to be nearly inactive over pure rutile and pure anatase, but very efficient on P25 and also on physical mixtures of anatase and rutile prepared via sonication in water. Many other studies have since described the improved activities of anatase–rutile composites, including P25, for different photocatalytic reactions and different anatase–rutile concentrations.[296–318]

Su et al. investigated TiO_2 films with varied anatase–rutile composition, but otherwise nearly identical properties in porosity, grain size and crystallinity.[319] The rate constant for MB degradation increased with anatase content starting from pure rutile ($k = 0.007$ h^{-1}, 30 mL MB solution [4 μmol L^{-1}], pH 7, 365 nm LED) indicating higher activity of anatase over rutile. When the anatase content was in the range of 40–80%, a clear synergistic effect on the photocatalytic rates was observed, increasing the rate constant of MB degradation significantly and off-trend (**Figure 11**). The observed rates in this composition range were far higher even than for pure anatase (up to $k = 0.071$ h^{-1}). The optimum composition was found at anatase:rutile 60:40%. At anatase contents higher than 80%, the rutile content was found to be too low for synergistic charge carrier separation, and the activity was simply dominated by the anatase phase.

Kho et al. varied the anatase–rutile composition in TiO_2 nanoparticles during synthesis via flame spray pyrolysis from 4–95 mol% anatase.[312] While all composites exhibited very similar surface areas and particle size, a maximum activity for H_2 generation from aqueous methanol (10 vol%) was found for composites containing 39% anatase (425 μmol h^{-1} per 0.1 g catalyst, 150 mL methanol/H_2O, 0.4 wt% Pt, 300 W Xe lamp). Moreover, only in-situ prepared mixtures showed high catalytic activity; physical mixtures of anatase and rutile in a 39:61 ratio did not show any synergistic effects due to lack of intimate physical contact (≈140 μmol h^{-1}). Additionally, the highly reducing hydroxymethyl radical (.CH_2OH) was identified

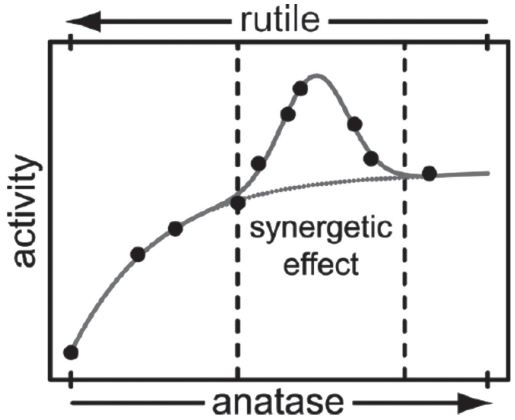

Figure 11. Increasing activity of anatase–rutile multiphase heterojunctions with identical properties but increasing anatase content, showing a clear synergistic effect between 40–80% anatase. Reproduced with permission.[319] Copyright 2011, American Chemical Society.

during methanol oxidation, which can inject additional electrons into the CB of TiO_2 (anatase or rutile). A mechanism for improved electron separation onto rutile was proposed being responsible for the high activities of the multiphase heterojunction.

In contrast, several research groups claim that the improved activity of anatase–rutile composites has nothing to do with a synergistic effect, rather that anatase and rutile actually exhibit the same photocatalytic activity, but their crystal surfaces have different capacity for the adsorption of O_2 necessary for the oxygen reduction step during aerobic degradation reactions, resulting in altered activities with changes in the anatase–rutile composition.[320] Ohtani et al. claim that anatase, rutile and small amounts of amorphous TiO_2 in P25 act completely independently during photocatalysis.[321]

In 1996, Kavan et al. determined that the CB of anatase lies 0.2 eV above the CB of rutile,[322] with rutile having E_g of ≈3.03 eV and anatase having E_g of 3.2 eV. These energetics favor charge carrier separation upon irradiation in a way that electrons are transferred to the rutile CB, and the holes to the VB of anatase. Kawahara et al. proved the interfacial electron transfer from anatase to rutile CB using patterned thin films.[323] By investigating the gas phase oxidation of acetaldehyde, a higher activity was found for anatase–rutile composites (k = 0.43 h^{-1}), compared to bare rutile exhibiting a reaction rate of (k = 0.005 h^{-1}). When the photodeposition of silver was investigated, silver depositions were found on rutile, proving the photoexcited electrons being transferred to rutile. Several later studies on multiphase TiO_2 heterojunctions of anatase–rutile further confirmed this behavior.[324,325] In contrast, Xiong et al. revealed by photoemission electron microscopy (PEEM) on anatase–rutile composite films that the rutile work function is 0.2 eV lower than that of anatase, which places the rutile CB edge higher than that of anatase,[326] which would result in photoexcited electrons being transferred to the anatase CB upon light irradiation of a rutile-anatase multiphase heterojunction. Several studies by EPR proved this mechanism to be valid,[292,327] and theoretical calculations underlined the experimental evidence proposing the photogenerated holes being transferred and accumulated simultaneously on rutile.[328] Carneiro et al., using experimental evidence from both time-resolved microwave conductance measurements and different photocatalytic activity studies, reported that photogenerated holes were trapped at the rutile surface in their anatase–rutile composites, indicating hole transfer from anatase to rutile.[329] Very recently, Scanlon et al. used density functional theory (DFT), hybrid quantum-mechanical/molecular-mechanical calculations and X-ray photoelectron spectroscopy (XPS) experiments to support the model of electron transfer from rutile to anatase CB and simultaneous hole transfer from anatase to rutile VB.[330] The VB edge of anatase was found to be ≈0.47 eV lower than the VB of rutile by modeling data, and additional XPS data revealed independently a comparable band offset of ≈0.39 eV (**Figure 12**). The high electron affinity of anatase results in photogenerated electrons being transferred from rutile on anatase, and thus acting as the driving force for improved photocatalytic activities of anatase–rutile multiphase heterojunctions.

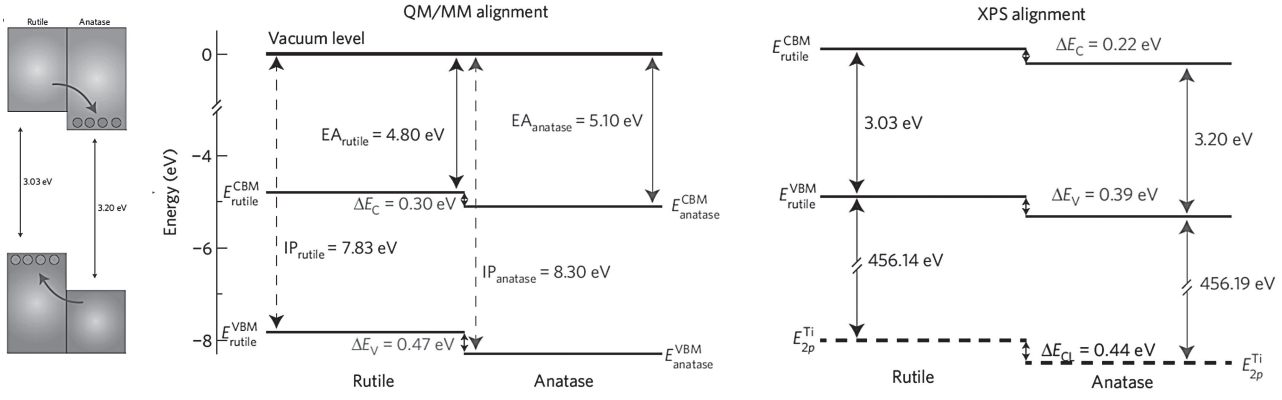

Figure 12. Band alignment in anatase–rutile multiphase heterojunctions estimated by quantum-mechanical/molecular-mechanical calculations and XPS measurements. Reproduced with permission.[330] Copyright 2013. Macmillan Publishers Limited.

The multiphase heterojunction between anatase-TiO_2 and brookite-TiO_2 has recently also gained some attention. Ozawa et al. prepared anatase–brookite composites with anatase content ranging from 55 to 100%.[331] The highest photocatalytic activity for acetaldehyde oxidation was found at a ratio of anatase:brookite of 65.3:34.6 (k = 1.40 h^{-1} m^{-2}, compared to k = 0.26 h^{-1} m^{-2} for pure anatase, 25 mg catalyst, 400 ppm acetaldehyde, 300 W Xe lamp). Yu et al. prepared hierarchical macro/mesoporous anatase–brookite composites via hydrothermal synthesis.[332] The trimodal porosity arising from anatase (brookite) nanocrystallite agglomerates resulted in surface area of 150–460 m^2 g^{-1}, and the anatase content was varied between 70–100%. The maximum photocatalytic activity for acetone oxidation was found at a ratio of anatase:brookite of 70:30 (k = 9.12 × 10^{-3} min^{-1}, $k \approx 2.5 \times 10^{-3}$ min^{-1} for pure anatase, 0.3 g catalyst, 400 ± 20 ppm acetone, 15 W UV (365 nm) lamp).

Kandiel et al. prepared brookite nanorods decorated with anatase nanoparticles in a one-step hydrothermal process using titanium bis(ammonium lactate) dihydroxide and urea.[333] The phase composition was tailored by changing the concentration of urea during synthesis and varied between 0–100% anatase. Brookite nanorods and anatase–brookite composites (72:28 %) showed higher activities in photocatalytic H_2 evolution (photonic efficiencies (H_2 production rate divided by photon flux) $\xi \approx$ 11.5% and 13%, respectively, 0.5 g L^{-1} catalyst, 75 mL methanol/H_2O solution [4.93 mol L^{-1}], 0.5 wt% Pt, 1000 W Xe lamp, UG1 filter) than pure anatase ($\xi \approx$ 7%) due to a 140 mV more negative flatband potential of brookite nanorods compared to anatase, leading to charge transfer in the composite of photoexcited electrons to the anatase CB. This observation was confirmed by Tay et al. who prepared anatase–brookite multiphase heterojunctions from TiS_2 and NaOH in a hydrothermal process.[334] In the photocatalytic DCA degradation however, anatase showed better activities ($\xi \approx$ 5.5% decreasing with brookite content and decreasing surface area, 30 mg catalyst, 60 mL KNO_3 solution [10 mmol L^{-1}], 1 mmol L^{-1} initial DCA concentration, 450 W Xe lamp, λ > 320 nm) due to its larger surface area. A subsequent calcination study (400–800 °C for 2 h) further tuned the phase composition of the thus-prepared materials.[335] As a result, multiphase heterojunctions of anatase–rutile, anatase–brookite, brookite–rutile, and anatase–brookite–rutile were prepared besides the phase-pure materials. The former synergistic effect between anatase and brookite was confirmed by photocatalytic methanol oxidation experiments, anatase–brookite nanoparticles showed higher activities ($\xi \approx$ 13.5%, 65 mg catalyst in 65 mL methanol/H_2O [30 mmol L^{-1}], 450 W Xe lamp, λ > 320 nm) than pure anatase nanoparticles ($\xi \approx$ 7%). Very small additional amounts of rutile (6 wt%) had no further effect, while larger amounts of rutile (49 wt%) reduced the activity drastically ($\xi \approx$ 6%), possibly due to disturbed charge transfer. However, pure brookite nanoparticles still exhibited higher photocatalytic activities ($\xi \approx$ 16%) compared to anatase or anatase-rich composites. Brookite–rutile composites showed no enhanced methanol oxidation ($\xi \approx$ 3–7.5%).

Zhao et al. investigated anatase–brookite multiphase heterojunctions in photocatalytic CO_2 reduction experiments.[336] Anatase-rich materials were more active than brookite-rich, the multiphase composite anatase:brookite 3:1 showed the highest reduction rates (0.21 μmol h^{-1} per 0.1 g catalyst, gas mixture of 97.7 vol% CO_2 and 2.3 vol% H_2O, 150 W solar simulator), which was higher than that of P25 (0.13 μmol h^{-1} per 0.1 g catalyst) and pure anatase (0.12 μmol h^{-1} per 0.1 g catalyst) or brookite materials (0.07 μmol h^{-1} per 0.1 g catalyst). However, the surface areas of the different composites were very different, ranging from 76.6 to 145.6 m^2 g^{-1}; after normalizing to the surface areas, composites with anatase:brookite ratio of 50:50 yielded the highest CO_2 reduction rates.

Very interesting examples of multiphase heterojunctions have been recently reported consisting of other, non-TiO_2 photocatalyst materials. For example, Wang et al. prepared a multiphase type II heterojunction of α-Ga_2O_3 and β-Ga_2O_3 by calcination, and reported significantly enhanced photocatalytic overall water splitting (H_2/O_2 up to 125/62 μmol h^{-1} m^{-2} per 0.5 g catalyst, 500 mL pure water, 2 wt% NiO_x co-catalyst, 450 W Hg lamp).[337] The optimum activity for the composites was obtained after calcination at 863 K. Pure α-Ga_2O_3 or β-Ga_2O_3 showed relatively low activities (40/20 and 15/7 μmol h^{-1} m^{-2}) per 0.5 g catalyst, respectively) compared to the multiphase heterojunctions. Transient absorption spectra and time-resolved infrared spectroscopy revealed ultra-fast charge carrier transfer and prolonged charge carrier lifetimes in α-Ga_2O_3–β-Ga_2O_3 composites in comparison to single-phase materials, which can be attributed to an efficient charge carrier transfer and separation across this type II heterojunction (**Figure 13**). Photoexcited electrons are transferred from the CB of α-Ga_2O_3 to β-Ga_2O_3, while the holes are accumulated and spatially separated in the VB of α-Ga_2O_3, reducing charge carrier recombination and enhancing photocatalytic activity.

A similar effect was observed in visible light-active α-Bi_2O_3 and β-Bi_2O_3.[338] Photoluminescence spectra showed reduced charge carrier recombination rates in the multiphase composite compared to pure β-Bi_2O_3, and the band positions of the different Bi_2O_3 phases were estimated from flatband potential and E_g measurements (Figure 13). The α-Bi_2O_3–β-Bi_2O_3 multiphase composite also forms a type II heterojunction with improved charge carrier separation and transfer, with electrons moving to the CB of β-Bi_2O_3 and holes to the VB of α-Bi_2O_3 upon light irradiation. Enhanced photocatalytic degradation rates for either RhB (up to k = 0.043 min^{-1}) or MO (up to k = 0.128 min^{-1}) were determined under visible light irradiation for the multiphase Bi_2O_3 heterojunction photocatalysts (0.2 g catalyst, 100 mL dye solution [1 x 10^{-4} mol L^{-1}], 300 W Xe lamp, λ > 420 nm) in comparison to the phase-pure β-Bi_2O_3 (k = 0.027 min^{-1} (RhB) and k = 0.063 min^{-1} (MO)). Sun et al. prepared a comparable type II multiphase heterojunction with Bi_2O_3, using α-Bi_2O_3 and γ-Bi_2O_3.[339] Improved photocatalytic RhB degradation in visible light was observed; 95% degradation was achieved after 1 hour, compared to 40% for α-Bi_2O_3 or γ-Bi_2O_3 (50 mg catalyst, 50 mL RhB solution [10^{-5} mol L^{-1}], 500 W Xe lamp, λ > 420 nm). The improved activity was explained by efficient transfer of electrons into the γ-Bi_2O_3 CB and holes into the α-Bi_2O_3 VB reducing recombination probability.

Tsang et al. prepared macroporous Ta_2O_5, TaON, and Ta_3N_5 using polystyrene spheres as templates for macroporous Ta_2O_5 followed by heat treatment in ammonia.[340] During ammonolysis, a multiphase heterojunction of β-TaON and γ-TaON (35:65%) was prepared, and subsequently used for H_2 evolution from aqueous ethanol (8.5 μmol h^{-1} per 0.04 g catalyst, 110 mL

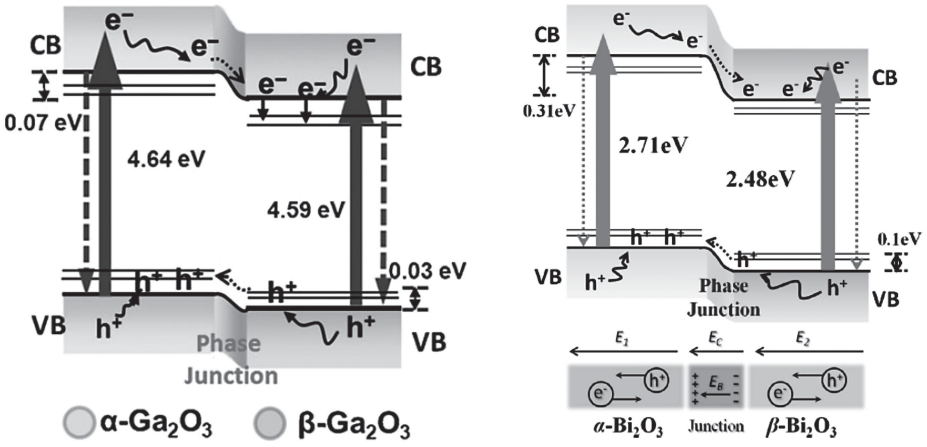

Figure 13. Left: Schematic illustration of charge carrier transfer and separation across α-Ga_2O_3 – β-Ga_2O_3. Reproduced with permission.[337] Copyright 2012, Wiley-VCH. Right: Charge carrier transfer and separation in visible light across α-Bi_2O_3–β-Bi_2O_3. Reproduced with permission.[338] Copyright 2013, Elsevier. Band positions are not comparable.

ethanol/H_2O [9 vol%], 300 W Xe lamp). Normalized for the surface area, the macroporous β-TaON/γ-TaON heterojunction generated more hydrogen under the same reaction conditions than the pure phase β-TaON, which was attributed to the charge separation in the composite material. Wang et al. prepared hollow urchin-like β-TaON/γ-TaON multiphase heterojunctions via hydrothermal synthesis of hollow urchin-like Ta_2O_5 also followed by annealing in ammonia.[341] γ-TaON and the β-TaON/γ-TaON composite showed significant activities for hydrogen generation under visible light irradiation (381.6 µmol/h and 351.9 µmol h^{-1} per 0.3 g catalyst, respectively, in 200 mL methanol/H_2O [10 vol%], 0.1 wt% Ru, 300 W Xe lamp, $\lambda > 420$ nm) with quantum efficiencies (Q.E.) of 9.5 and 8.7%, respectively. Additionally, the multiphase composite showed higher activity than the phase-pure β-TaON (287.7 µmol h^{-1} per 0.3 g catalyst, Q.E. 6.9%).

5. Conclusion

Forming multiphase or multicomponent heterojunctions of photocatalysts is a very promising strategy to improve photocatalytic activity by enhanced charge carrier separation and thus reduced recombination. By carefully choosing the relative band positions of the two/three photocatalysts, very effective charge separation can be achieved. In the best cases vectorial charge transfer is achieved, guiding electrons to the surface of the desired phase of the composite photocatalyst. By selectively decorating those surfaces with co-catalysts, the most active heterojunctions can be realized. Besides improved charge carrier separation, the other obvious motivation preparing multicomponent heterojunctions is the extension of light absorption by the combination of at least one visible light absorbing semiconductor with another semiconductor material. Many effective examples have been reported to expand the light absorption by this strategy deep into the visible light range.

However, it seems difficult to predict the extent of photocatalytic activity of a multiphase or multicomponent heterojunction just by the relative band positions. In some examples shown, the photocatalytic activity was improved strongly even when the difference in, for example, CB minimum was only minor. Examples are the multiphase heterojunctions of the different TiO_2 phases. On the other hand, in some cases the activity was only slightly improved in relation to the big difference in band positions (e.g., Cu_2O/TiO_2). One reason for this effect might be the different electron mobility in different components, but this has to be proven. Unfortunately, often the molar/weight ratio between the two components of a heterojunction is also not reported, which makes a reliable comparison very difficult, too. Moreover, the lack of standardized photocatalytic and photoelectrochemical measurements and their protocols remains a key issue to reliably compare photocatalytic results.[342]

Given the examples in this review of the demonstrated enhanced photoactivity enabled by photocatalyst heterojunctions, one might question the purpose of aiming for phase pure materials. Indeed, photocatalysts containing "impurities", either in the form of another crystal phase or deliberately added second (or third) material, always seem to have higher photocatalytic activities than the respective pure compounds. Is a pure photocatalytic material actually worthy of investigation (beyond the purposes of determining the baseline characteristics of the phase-pure materials), or should one always aim for a "non-pure" material when attempting to develop superior photocatalysts? The challenge is to prove that a material is actually 100 % phase pure, and/or actually needs to be. Designing semiconductor composites might be the better path to find the most active photocatalyst systems.

In any case, photocatalysis researchers have to pay much more careful attention to their materials characterization, particularly concerning crystal phase analysis. The biggest challenge lies in analyzing the amounts of "impurity" phase(s), or even amorphous phases. Especially very high activities should be followed by a detailed investigation of the origin of the photocatalytic activity, and questions of phase purity and multiphase composition should be of constant and utmost concern. Consequently, by careful tailoring the phase compositions and investigating the influence of every phase, optimum ratios and interfacial contacts can be established to maximize

photocatalytic activity for every heterojunction. For many of the presented heterojunctions, such investigations have not been yet performed. Moreover, facile and reproducible synthesis conditions are necessary to tune phase compositions carefully. Sol-gel techniques should be most suitable to tune precursor ratios influencing the resulting multiphase compounds.

Finally, surprisingly very few examples in literature pay adequate attention to the formation of p/n-type heterojunctions simultaneously. Forming a multiphase or multicomponent heterojunction usually increases photocatalytic activity as shown in this review, but forming heterojunctions of n-type semiconductors with p-type semiconductors would further enhance charge separation and open up new possibilities for vectorial charge transfer. The BiOI-TiO_2 system is a very good example, in which visible-light excited electrons are transferred to TiO_2 after contact, and do not remain in the CB of BiOI.[133] Electrochemical investigations to determine the semiconductor behavior should be a major concern in the future for materials scientists in pursuit of designing new and more efficient heterojunction systems. The investigation of band positions after contact and to find experimental evidence for the p–n junction will be important in the future. However, forming photocatalytic or photoelectrochemical p/n-type heterojunctions might be a viable strategy to make, for example, photoelectrochemical water splitting an economic alternative to electrolysis, and may be integral to the design of more efficient photocatalyst systems.

Acknowledgements

The author would like to thank Prof. Lianzhou Wang and Prof. Gao Qing (Max) Lu from The University of Queensland for the excellent collaboration throughout the last years, and Dr. Jeremy J. Pietron (US Naval Research Laboratory, Washington, DC) and Prof. Bernd M. Smarsly (Justus-Liebig-University Giessen) for many valuable discussions and support. The author would also like to thank Prof. Michael Wark (Carl von Ossietzky University Oldenburg) for many fruitful discussions, his constant support and manifold scientific contributions in the last years. The German Research Foundation DFG is gratefully acknowledged for funding in the Emmy-Noether program (MA 5392/3–1).

Received: September 17, 2013
Revised: November 6, 2013
Published online: December 18, 2013

[1] N. S. Lewis, D. G. Nocera, *Proc. Natl. Acad. Sci. U. S. A.* **2006**, *103*, 15729.
[2] F. E. Osterloh, *Chem. Mater.* **2007**, *20*, 35.
[3] A. Kudo, Y. Miseki, *Chem. Soc. Rev.* **2009**, *38*, 253.
[4] X. Chen, S. Shen, L. Guo, S. S. Mao, *Chem. Rev.* **2010**, *110*, 6503.
[5] K. Maeda, K. Domen, *J. Phys. Chem. Lett.* **2010**, *1*, 2655.
[6] K. Maeda, *J. Photochem. Photobiol. C: Photochem. Rev.* **2011**, *12*, 237.
[7] F. E. Osterloh, *Chem. Soc. Rev.* **2013**, *42*, 2294.
[8] O. K. Varghese, M. Paulose, T. J. LaTempa, C. A. Grimes, *Nano Lett.* **2009**, *9*, 731.
[9] S. N. Habisreutinger, L. Schmidt-Mende, J. K. Stolarczyk, *Angew. Chem. Int. Ed.* **2013**, *52*, 7372.
[10] P. Wardman, *J. Phys. Chem. Ref. Data* **1989**, *18*, 1637.
[11] M. R. Hoffmann, S. T. Martin, W. Choi, D. W. Bahnemann, *Chem. Rev.* **1995**, *95*, 69.
[12] H. Kisch, *Angew. Chem. Int. Ed.* **2012**, *51*, 2.
[13] S. Sakthivel, M. V. Shankar, M. Palanichamy, B. Arabindoo, D. W. Bahnemann, V. Murugesan, *Water Res.* **2004**, *38*, 3001.
[14] A. A. Ismail, S. A. Al-Sayari, D. W. Bahnemann, *Catal. Today* **2013**, *209*, 2.
[15] O. Merka, D. W. Bahnemann, M. Wark, *ChemCatChem* **2012**, *4*, 1819.
[16] V. Artero, M. Chavarot-Kerlidou, M. Fontecave, *Angew. Chem. Int. Ed.* **2011**, *50*, 7238.
[17] M. Wang, L. Chen, L. Sun, *Energy Environ. Sci.* **2012**, *5*, 6763
[18] P. D. Tran, L. Xi, S. K. Batabyal, L. H. Wong, J. Barber, J. S. C. Loo, *Phys. Chem. Chem. Phys.* **2012**.
[19] X. Zong, H. Yan, G. Wu, G. Ma, F. Wen, L. Wang, C. Li, *J. Am. Chem. Soc.* **2008**, *130*, 7176.
[20] K. Maeda, D. Lu, K. Teramuraxa, K. Domen, *J. Mater. Chem.* **2008**, *18*, 3539.
[21] K. Maeda, T. Ohno, K. Domen, *Chem. Sci.* **2011**, *2*, 1362.
[22] D. Wang, R. Li, J. Zhu, J. Shi, J. Han, X. Zong, C. Li, *J. Phys. Chem. C* **2012**, *116*, 5082.
[23] M. W. Kanan, D. G. Nocera, *Science* **2008**, *321*, 1072.
[24] C. Ding, J. Shi, D. Wang, Z. Wang, N. Wang, G. Liu, F. Xiong, C. Li, *Phys. Chem. Chem. Phys.* **2013**, *15*, 4589.
[25] Y. P. Xie, G. Liu, G. Q. (Max) Lu, H.-M. Cheng, *Nanoscale* **2012**, *4*, 1267.
[26] J. Yang, D. Wang, H. Han, C. Li, *Acc. Chem. Res.* **2013**, *46*, 1900.
[27] P. V. Kamat, *J. Phys. Chem. Lett.* **2011**, *2*, 242.
[28] K. S. Novoselov, A. K. Geim, S. V. Morozov, D. Jiang, Y. Zhang, S. V. Dubonos, I. V. Grigorieva, A. A. Firsov, *Science* **2004**, *306*, 666.
[29] X. Huang, X. Qi, F. Boey, H. Zhang, *Chem. Soc. Rev.* **2012**, *41*, 666.
[30] Q. Xiang, J. Yu, *J. Phys. Chem. Lett.* **2013**, *4*, 753.
[31] L.-L. Tan, S.-P. Chai, A. R. Mohamed, *Chem. Sus. Chem.* **2012**, *5*, 1868.
[32] W. Tu, Y. Zhou, Z. Zou, *Adv. Funct. Mater.* **2013**, *23*, 4996.
[33] G. Xie, K. Zhang, B. Guo, Q. Liu, L. Fang, J. R. Gong, *Adv. Mater.* **2013**, *25*, 3820.
[34] W. Choi, A. Termin, M. R. Hoffmann, *J. Phys. Chem.* **1994**, *98*, 13669.
[35] J. Z. Bloh, R. Dillert, D. W. Bahnemann, *J. Phys. Chem. C* **2012**, *116*, 25558.
[36] F. Wang, C. Di Valentin, G. Pacchioni, *ChemCatChem* **2012**, *4*, 476.
[37] R. Asahi, T. Morikawa, T. Ohwaki, K. Aoki, Y. Taga, *Science* **2001**, *293*, 269.
[38] R. Marschall, L. Wang, *Catal. Today* **2013**, DOI: 10.1016/j.cattod.2013.10.088.
[39] S. Linic, P. Christopher, D. B. Ingram, *Nat. Mater.* **2011**, *10*, 911.
[40] P. Wang, B. Huang, Y. Dai, M.-H. Whangbo, *Phys. Chem. Chem. Phys.* **2012**, *14*, 9813.
[41] W. Hou, S. B. Cronin, *Adv. Funct. Mater.* **2013**, *23*, 1612.
[42] P. A. DeSario, J. J. Pietron, D. E. DeVantier, T. H. Brintlinger, R. M. Stroud, D. R. Rolison, *Nanoscale* **2013**, *5*, 8073.
[43] C. Das, P. Roy, M. Yang, H. Jha, P. Schmuki, *Nanoscale* **2011**, *3*, 3094.
[44] S. Hoang, T. Q. Ngo, S. P. Berglund, R. R. Fullon, J. G. Ekerdt, C. B. Mullins, *ChemPhysChem* **2013**, *14*, 2270.
[45] G. Liu, L. Wang, C. Sun, X. Yan, X. Wang, Z. Chen, S.C. Smith, H.-M. Cheng, G. Q. Lu, *Chem. Mater.* **2009**, *21*, 1266.
[46] A. Mukherji, R. Marschall, A. Tanksale, C. Sun, S.C. Smith, L. Wang, G. Q. (Max) Lu, *Adv. Funct. Mater.* **2011**, *21*, 126.
[47] R. Marschall, A. Mukherji, A. Tanksale, C. Sun, S.C. Smith, L. Wang, G.Q. (Max) Lu, *J. Mater. Chem.* **2011**, *21*, 8871.
[48] X. Zong, C. Sun, Z. Chen, A. Mukherji, H. Wu, J. Zou, S. C. Smith, G. Q. Lu, L. Wang, *Chem. Commun.* **2011**, *47*, 6293.
[49] M. K. Nazeeruddin, R. Splivallo, P. Liska, P. Comte, M. Grätzel, *Chem. Commun.* **2003**, 1456.

[50] H. G. Yang, C. Sun, S. Z. Qiao, J. Zou, G. Liu, S. C. Smith, H.-M. Cheng, G. Q. Lu, *Nature* **2008**, *453*, 638.
[51] G. Liu, J. C. Yu, G. Q. (Max) Lu, H.-M. Cheng, *Chem. Commun.* **2011**, *47*, 6763.
[52] M. Batzill, *Energy Environ. Sci.* **2011**, *4*, 3275.
[53] S. He, S. Zhang, J. Lu, Y. Zhao, J. Ma, M. Wei, D. G. Evansa, X. Duan, *Chem. Commun.* **2011**, *47*, 10797.
[54] D. Zhang, S. Wang, J. Zhu, H. Li, Y. Lu, *Appl. Catal. B* **2012**, *123–124*, 398.
[55] Y. Zhao, F. Pan, H. Li, T. Niu, G. Xua, W. Chen, *J. Mater. Chem. A* **2013**, *1*, 7242.
[56] M. O. Watanabe, J. Yoshida, M. Mashita, T. Nakanisi, A. Hojo, *J. Appl. Phys.* **1985**, *57*, 5340.
[57] N. Serpone, E. Borgarello, M. Grätzel, *J. Chem. Soc., Chem. Commun.* **1984**, 342.
[58] L. Spanhel, H. Weller, A. Henglein, *J. Am. Chem. Soc.* **1987**, *109*, 6632.
[59] S. Hotchandani, P. V. Kamat, *J. Phys. Chem.* **1992**, *96*, 6834.
[60] K. R. Gopidas, M. Bohorquez, P. V. Kamat, *J. Phys. Chem.* **1990**, *94*, 6435.
[61] J. E. Evans, K. W. Springer, J. Z. Zhang, *J. Chem. Phys.* **1994**, *101*, 6222.
[62] P. V. Kamat, *J. Phys. Chem. C* **2008**, *112*, 18737, and references within.
[63] H. Gerischer, M. Lübke, *J. Electroanal. Chem. Interfacial Electrochem.* **1986**, *204*, 225.
[64] R. Vogel, K. Pohl, H. Weller, *Chem. Phys. Lett.* **1990**, *174*, 241.
[65] S. Kohtani, A. Kudo, T. Sakata, *Chem. Phys. Lett.* **1993**, *206*, 166.
[66] S. Hotchandani, P. V. Kamat, *Chem. Phys. Lett.* **1992**, *191*, 320.
[67] J. Yoshimura, A. Kudo, A. Tanaka, K. Domen, K. Maruya, T. Onishi, *Chem. Phys. Lett.* **1988**, *147*, 401.
[68] R. Kietzmann, F. Willig, H. Weller, R. Vogel, D. N. Nath, R. Eichberger, P. Liska, J. Lehnert, *Mol. Cryst. Liq. Cryst.* **1991**, *194*, 169.
[69] L. Spanhel, A. Henglein, H. Weller, *Ber. Bunsen-Ges. Phys. Chem.* **1987**, *91*, 1359.
[70] J. Rabani, *J. Phys. Chem.* **1989**, *93*, 7707.
[71] P. V. Kamat, B. Patrick, *J. Phys. Chem.* **1992**, *96*, 6829.
[72] A. R. Kortan, R. Hull, R. L. Opila, M. G. Bawendi, M. L. Steigerwald, P. J. Carroll, L. E. Brus, *J. Am. Chem. Soc.* **1990**, *112*, 1327.
[73] Y. Tian, T. Newton, N. A. Kotov, D. M. Guldi, J. H. Fendler, *J. Phys. Chem.* **1996**, *100*, 8927.
[74] R. Vogel, P. Hoyer, H. Weller, *J. Phys. Chem.* **1994**,*98*, 3183.
[75] I. Bedja, P. V. Kamat, *J. Phys. Chem.* **1995**, *99*, 9182.
[76] K. Vinodgopal, I. Bedja, P. V. Kamat, *Chem. Mater.* **1996**, *8*, 2180.
[77] T. Hirai, K. Suzuki, I. Komasawa, *J. Colloid Int. Sci.* **2001**, *244*, 262.
[78] P. A. Santz, P. V. Kamat, *Phys. Chem. Chem. Phys.* **2002**, *4*, 198
[79] J. C. Kim, J. Choi, Y. B. Lee, J. H. Hong, J. I. Lee, J. W. Yang, W. I. Lee, N. H. Hur, *Chem. Commun.* **2006**, 5024.
[80] D. R. Baker, P. V. Kamat, *Adv. Funct. Mater.* **2009**, *19*, 805.
[81] H. Park, W. Choi, M. R. Hoffmann, *J. Mater. Chem.* **2008**, *18*, 2379.
[82] W.-T. Sun, Y. Yu, H.-Y. Pan, X.-F. Gao, Q. Chen, L.-M. Peng, *J. Am. Chem. Soc.* **2008**, *130*, 1124.
[83] T. Kiyonaga, T. Akita, H. Tada, *Chem. Commun.* **2009**, 2011.
[84] J. Li, M. W. G. Hoffmann, H. Shen, C. Fabrega, J. D. Prades, T. Andreu, F. Hernandez-Ramirez, S. Mathur, *J. Mater. Chem.* **2012**, *22*, 20472.
[85] M. Law, L. E. Greene, A. Radenovic, T. Kuykendall, J. Liphardt, P. Yang, *J. Phys. Chem. B* **2006**, *110*, 22652.
[86] L. Wu, J. Xing, Y. Hou, F. Y. Xiao, Z. Li, H. G. Yang, *Chem. Eur. J.* **2013**, *19*, 8393.
[87] K. Y. Song, M. K. Park, Y. T. Kwon, H. W. Lee, W. J. Chung, W. I. Lee, *Chem. Mater.* **2001**, *13*, 2349.
[88] R. Ostermann, S. Sallard, B. M. Smarsly, *Phys. Chem. Chem. Phys.* **2009**, *11*, 3648.
[89] A. Srinivasan, M. Miyauchi, *J. Phys. Chem. C* **2012**, *116*, 15421.
[90] B. Lu, X. Li, T. Wang, E. Xie, Z. Xu, *J. Mater. Chem. A* **2013**, *1*, 3900.
[91] M. Grandcolas, T. Cottineau, A. Louvet, N. Keller, V. Keller, *Appl. Catal. B* **2013**, *138–139*, 128.
[92] E. Karacsonyi, L. Baia, A. Dombi, V. Danciu, K. Mogyorosi, L. C. Pop, G. Kovacs, V. Cosoveanu, A. Vulpoi, S. Simon, Z. Pap, *Catal. Today* **2013**, *208*, 19.
[93] C. Wang, F. Jiang, R. Zhou, Y. Dua, P. Yang, C. Wang, J. Xu, *Mater. Res. Bull.* **2013**, *48*, 1099.
[94] N. A. Ramos-Delgado, L. Hinojosa-Reyes, I. L. Guzman-Mar, M. A. Gracia-Pinilla, A. Hernandez-Ramirez, *Catal. Today* **2013**, *209*, 35.
[95] C. W. Lai, S. Sreekantan, *Int. J. Hydrogen Energy* **2013**, *38*, 2156.
[96] F. Ribonia, L. G. Bettini, D. W. Bahnemann, E. Selli, *Catal. Today* **2013**, *209*, 28.
[97] L. A. King, W. Zhao, M. Chhowalla, D. J. Riley, G. Eda, *J. Mater. Chem. A* **2013**, *1*, 8935.
[98] W. Zhou, Z. Yin, Y. Du, X. Huang, Z. Zeng, Z. Fan, H. Liu, J. Wang, H. Zhang, *Small* **2013**, *9*, 140.
[99] Y. C. Liu, J. G. L. Griffin, S. S. Chan, I. E. Wachs, *J. Catal.* **1985**, *94*, 108.
[100] B. J. Ma, J. S. Kim, C. H. Choi, S. I. Woo, *Int. J. Hydrogen Energy* **2013**, *38*, 3582.
[101] S. Furukawa, T. Shishido, K. Teramura, T. Tanaka, *ACS Catal.* **2012**, *2*, 175.
[102] H.-N. Kim, J. H. Moon, *ACS Appl. Mater. Interfaces* **2012**, *4*, 5821.
[103] Y. Bessekhouad, D. Robert, J.-V. Weber, *Catal. Today* **2005**, *101*, 315.
[104] Z. Bian, J. Zhu, S. Wang, Y. Cao, X. Qian, H. Li, *J. Phys. Chem. C* **2008**, *112*, 6258.
[105] K. Su, Z. Ai, L. Zhang, *J. Phys. Chem. C* **2012**, *116*, 17118.
[106] S. K. Poznyak, D. V. Talapin, A. I. Kulak, *J. Phys. Chem. B* **2001**, *105*, 4816.
[107] D. Shchukin, S. Poznyak, A. Kulak, P. Pichat, *J. Photochem. Photobiol. A* **2004**, *162*, 423.
[108] V. Rodríguez-González, A. Moreno-Rodríguez, M. May, F. Tzompantzi, R. Gómez, *J. Photochem. Photobiol. A* **2008**, *193*, 266.
[109] J. Mu, B. Chen, M. Zhang, Z. Guo, P. Zhang, Z. Zhang, Y. Sun, C. Shao, Y. Liu, *ACS Appl. Mater. Interfaces* **2012**, *4*, 424.
[110] S. Pavasupreea, Y. Suzukia, S. Pivsa-Artb, S. Yoshikawa, *J. Solid State Chem.* **2005**, *178*, 128.
[111] I. Alessandri, M. Zucca, M. Ferroni, E. Bontempi, L. E. Depero, *Small* **2009**, *5*, 336.
[112] J. Tian, Y. Sang, Z. Zhao, W. Zhou, D. Wang, X. Kang, H. Liu, J. Wang, S. Chen, H. Cai, H. Huang, *Small* **2013**, *9*, 3864.
[113] N. Siedl, M. J. Elser, J. Bernardi, O. Diwald, *J. Phys. Chem. C* **2009**, *113*, 15792.
[114] A. Kambur, G. S. Pozan, I. Boz, *Appl. Catal. B* **2012**, *115–116*, 149.
[115] Y. Wang, Y. R. Su, L. Qiao, L. X. Liu, Q. Su, C. Q. Zhu, X. Q. Liu, *Nanotechnology* **2011**, *22*, 225702.
[116] M. Gurulakshmi, M. Selvaraj, A. Selvamani, P. Vijayan, N. R. S. Rekha, K. Shanthi, *Appl. Catal. A* **2012**, *449*, 31.
[117] S. Martha, D. P. Das, N. Biswal, K. M. Parida, *J. Mater. Chem.* **2012**, *22*, 10695.
[118] N. Siedl, S. O. Baumann, M. J. Elser, O. Diwald, *J. Phys. Chem. C* **2012**, *116*, 22967.
[119] T. H. Jeon, W. Choi, H. Park, *J. Phys. Chem. C* **2011**, *115*, 7134.
[120] K. E. deKrafft, C. Wang, W. Lin, *Adv. Mater.* **2012**, *24*, 2014.
[121] A. J. Cowan, C. J. Barnett, S. R. Pendlebury, M. Barroso, K. Sivula, M. Grätzel, J. R. Durrant, D. R. Klug, *J. Am. Chem. Soc.* **2011**, *133*, 10134.
[122] F. Mou, L. Xu, H. Ma, J. Guan, D. Chen, S. Wang, *Nanoscale* **2012**, *4*, 4650.
[123] S.S. Lee, H. Bai, Z. Liu, D.D. Sun, *Appl. Catal. B* **2013**, *140–141*, 68.

[124] N. Helaïli, Y. Bessekhouad, A. Bouguelia, M. Trari, *J. Hazard. Mater.* **2009**, *168*, 484.
[125] J. Zhang, H. Zhu, S. Zheng, F. Pan, T. Wang, *ACS Appl. Mater. Interfaces* **2009**, *1*, 2111.
[126] L. Yang, S. Luo, Y. Li, Y. Xiao, Q. Kang, Q. Cai, *Environ. Sci. Technol.* **2010**, *44*, 7641.
[127] Y. Wang, Y. Zhang, G. Zhao, H. Tian, H. Shi, T. Zhou, *ACS Appl. Mater. Interfaces* **2012**, *4*, 3965.
[128] C. Gao, J. Li, Z. Shan, F. Huang, H. Shen, *Mater. Chem. Phys.* **2012**, *122*, 183.
[129] S. K. Sarkar, J. Y. Kim, D. N. Goldstein, N. R. Neale, K. Zhu, C. M. Elliott, A. J. Frank, S. M. George, *J. Phys. Chem. C* **2010**, *114*, 8032.
[130] B. Chai, T. Peng, P. Zeng, J. Mao, *J. Mater. Chem.* **2011**, *21*, 14587.
[131] J. Wang, X. Li, X. Li, J Zhu, H. Li, *Nanoscale* **2013**, *5*, 1876.
[132] X. Zhang, L. Zhang, T. Xie, D. Wang, *J. Phys. Chem. C* **2009**, *113*, 7371.
[133] G. Dai, J. Yu, G. Liu, *J. Phys. Chem. C* **2011**, *115*, 7339.
[134] S. Peng, Y. Wu, P. Zhu, V. Thavasi, S. Ramakrishna, S. G. Mhaisalkar, *J. Mater. Chem.* **2011**, *21*, 15718.
[135] G. Tian, Y. Chen, H.-L. Bao, X. Meng, K. Pan, W. Zhou, C. Tian, J.-Q. Wang, H. Fu, *J. Mater. Chem.* **2012**, *22*, 2081.
[136] X. Wang, Y. Tang, Z. Chen, T.-T. Lim, *J. Mater. Chem.* **2012**, *22*, 23149.
[137] Y. Hou, X. Li, Q. Zhao, X. Quan, G. Chen, *J. Mater. Chem.* **2011**, *21*, 18067.
[138] M. Shang, W. Wang, L. Zhang, S. Sun, L. Wang, L. Zhou, *J. Phys. Chem. C* **2009**, *113*, 14727.
[139] G. Colón, S. Murcia López, M. C. Hidalgo, J. A. Navío, *Chem. Commun.* **2010**, *46*, 4809.
[140] Q.C. Xu, Y. H. Ng, Y. Zhang, J. S. C. Loo, R. Amal, T. T. Y. Tan, *Chem. Commun.* **2011**, *47*, 8641.
[141] J. Xu, W. Wang, S. Sun, L. Wang, *Appl. Catal. B* **2012**, *111–112*, 126.
[142] S. Obregón, G. Colón, *Appl. Catal. B* **2013**, *140–141*, 299.
[143] M. Zhang, C. Shao, J. Mu, Z. Zhang, Z. Guo, P. Zhang, Y. Liu, *Cryst. Eng. Commun.* **2012**, *14*, 605.
[144] G. Tian, Y. Chen, R. Zhai, J. Zhou, W. Zhou, R. Wang, K. Pan, C. Tiana, H. Fu, *J. Mater. Chem. A* **2013**, *1*, 6961.
[145] G. Xiao, X. Wang, D. Li, X. Fu, *J. Photochem. Photobiol. A* **2008**, *193*, 213.
[146] Z. He, Q. Xu, T. T. Yang Tan, *Nanoscale* **2011**, *3*, 4977.
[147] Y. Hu, D. Li, Y. Zheng, W. Chen, Y. He, Y. Shao, X. Fu, G. Xiao, *Appl. Catal. B* **2011**, *104*, 30.
[148] W. Yao, B. Zhang, C. Huang, C. Ma, X. Song, Q. Xu, *J. Mater. Chem.* **2012**, *22*, 4050.
[149] W. Teng, X. Li, Q. Zhao, G. Chen, *J. Mater. Chem. A* **2013**, *1*, 9060.
[150] J. Hou, Z. Wang, S. Jiao, H. Zhu, *J. Hazard. Mater.* **2011**, *192*, 1772.
[151] K. Li, B. Chai, T. Peng, J. Mao, L. Zan, *ACS Catal.* **2013**, *3*, 170.
[152] S.-Z. Kang, Y.-K. Yang, W. Bu, J. Mu, *J. Solid State Chem.* **2009**, *182*, 2972.
[153] J. S. Jang, S. J. Hong, J. Y. Kim, J. S. Lee, *Chem. Phys. Lett.* **2009**, *475*, 78.
[154] B.-X. Lei, W. Sun, Z.-F. Sun, *Mater. Res. Bull.* **2013**, *48*, 3625.
[155] Z. Xiong, X. S. Zhao, *J. Am. Chem. Soc.* **2012**, *134*, 5754.
[156] Z. Xiong, X. S. Zhao, *J. Mater. Chem. A* **2013**, *1*, 7738.
[157] X. Fan, B. Lin, H. Liu, L. He, Y. Chen, B. Gao, *Int. J. Hydrogen Energy* **2013**, *38*, 832.
[158] T. Cao, Y. Li, C. Wang, Z. Zhang, M. Zhang, C. Shao, Y. Liu, *J. Mater. Chem.* **2011**, *21*, 6922.
[159] S. B. Rawal, S. Bera, W. I. Lee, *Catal. Lett.* **2012**, *142*, 1482.
[160] W. Wang, S. Li, Y. Wen, M. Gong, L. Zhang, Y. Yao, Y. Chen, *Acta Phys. Chim. Sin.* **2008**, *24*, 1761.
[161] X. Lü, J. Liu, J. Zhu, D. Jiang, J. Xie, *J. Mater. Res.* **2010**, *25*, 104.
[162] H. Bai, Z. Liu, D. D. Sun, *Int. J. Hydrogen Energy* **2012**, *37*, 13998.
[163] W. Smith, H. Fakhouri, J. Pulpytel, S. Mori, R. Grilli, M. A. Baker, F. Arefi-Khonsari, *J. Phys. Chem. C* **2012**, *116*, 15855.
[164] Z. Zhao, J. Tian, D. Wang, X. Kang, Y. Sang, H. Liu, J. Wang, S. Chen, R. I. Boughton, H. Jiang, *J. Mater. Chem.* **2012**, *22*, 23395.
[165] S. S. Lee, H. Bai, Z. Liu, D. D. Sun, *Int. J. Hydrogen Energy* **2012**, *37*, 10575.
[166] J. Papp, S. Soled, K. Dwight, A. Wold, *Chem. Mater.* **1994**, *6*, 496.
[167] L. Li, L. Xu, W. Shi, J. Guan, *Int. J. Hydrogen Energy* **2013**, *38*, 816.
[168] H. Yu, R. Liu, X. Wang, P. Wang, J. Yu, *Appl. Catal. B* **2012**, *111–112*, 326.
[169] L. Zhu, B. Wei, L. Xu, Z. Lü, H. Zhang, H. Gao, J. Che, *Cryst. Eng. Commun.* **2012**, *14*, 5705.
[170] J. Guo, S. Ouyang, P. Li, Y. Zhang, T. Kako, J. Ye, *Appl. Catal. B* **2013**, *134–135*, 286.
[171] L. Kong, Z. Jiang, H.H. Lai, R.J. Nicholls, T. Xiao, M. O. Jones, P. P. Edwards, *J. Catal.* **2012**, *293*, 116.
[172] R. Guo, G. Zhang, J. Liu, *Mater. Res. Bull.* **2013**, *48*, 1857.
[173] B. Wen, X.-H. Wang, J. Lu, J.-L. Cao, Z.-S. Wang, *Mater. Res. Bull.* **2013**, *48*, 1806.
[174] R. Marschall, J. Soldat, G. W. Busser, M. Wark, *Photochem. Photobiol. Sci.* **2013**, *12*, 671.
[175] Y.-S. Xu, W.-D. Zhang, *Appl. Catal. B* **2013**, *140–141*, 306.
[176] H. Fan, H. Li, B. Liu, Y. Lu, T. Xie, D. Wang, *ACS Appl. Mater. Interfaces* **2012**, *4*, 4853.
[177] X. Lin, J. Xing, W. Wang, Z. Shan, F. Xu, F. Huang, *J. Phys. Chem. C* **2007**, *111*, 18288.
[178] Y.-S. Xu, Z.-J. Zhang, W.-D. Zhang, *Mater. Res. Bull.* **2013**, *48*, 1420.
[179] S. Balachandran, M. Swaminathan, *J. Phys. Chem. C* **2012**, *116*, 26306.
[180] X. Li, R. Huang, Y. Hu, Y. Chen, W. Liu, R. Yuan, Z. Li, *Inorg. Chem.* **2012**, *51*, 6245.
[181] H. Cheng, B. Huang, X. Qin, X. Zhang, Y. Dai, *Chem. Commun.* **2012**, *48*, 97.
[182] Z. Zhang, W. Wang, L. Wang, S. Sun, *ACS Appl. Mater. Interfaces* **2012**, *4*, 593.
[183] Y. Li, Y. Liu, J. Wang, E. Uchaker, Q. Zhang, S. Sun, Y. Huang, J. Li, G. Cao, *J. Mater. Chem. A* **2013**, *1*, 7949.
[184] S. Y. Chai, Y. J. Kim, M. H. Jung, A. K. Chakraborty, D. Jung, W. I. Lee, *J. Catal.* **2009**, *262*, 144.
[185] K. H. Reddy, S. Martha, K. M. Parida, *Inorg. Chem.* **2013**, *52*, 6390.
[186] S. Wu, H. Zheng, Y. Lian, Y. Wu, *Mater. Res. Bull.* **2013**, *48*, 2901.
[187] P. Madhusudana, J. Rana, J. Zhanga, J. Yua, G. Liu, *Appl. Catal. B* **2011**, *110*, 286.
[188] S. K. Pilli, T. G. Deutsch, T. E. Furtak, L. D. Brown, J. A. Turner, A. M. Herring, *Phys. Chem. Chem. Phys.* **2013**, *15*, 3273.
[189] R. Saito, Y. Miseki, K. Sayama, *Chem. Commun.* **2012**, *48*, 3833.
[190] J.A. Seabold, K.-S. Choi, *J. Am. Chem. Soc.* **2012**, *134*, 2186.
[191] H. W. Jeong, T. H. Jeon, J. S. Jang, W. Choi, H. Park, *J. Phys. Chem. C* **2013**, *117*, 9104.
[192] W. Wang, X. Huang, S. Wu, Y. Zhou, L. Wang, H. Shi, Y. Liang, B. Zou, *Appl. Catal. B* **2013**, *134–135*, 293.
[193] W. Zhao, Y. Wang, Y. Yang, J. Tang, Y. Yang, *Appl. Catal. B* **2012**, *115–116*, 90.
[194] J. Su, X.-X. Zou, G.-D. Li, X. Wei, C. Yan, Y.-N. Wang, J. Zhao, L.-J. Zhou, J.-S. Chen, *J. Phys. Chem. C* **2011**, *115*, 8064.
[195] H. Li, S. Yin, Y. Wang, T. Sato, *Appl. Catal. B* **2013**, *132–133*, 487.
[196] E.S. Kim, N. Nishimura, G. Magesh, J. Y. Kim, J.-W. Jang, H. Jun, J. Kubota, K. Domen, J. S. Lee, *J. Am. Chem. Soc.* **2013**, *135*, 5375.
[197] J. Cao, J. Xing, Y. Zhang, H. Tong, Y. Bi, T. Kako, M. Takeguchi, J. Ye, *Langmuir* **2013**, *29*, 3116.
[198] H. G. Kim, P. H. Borse, J. S. Jang, E. D. Jeong, O.-S. Jung, Y. J. Suh, J. S. Lee, *Chem. Commun.* **2009**, 5889.
[199] H. G. Kim, P. H. Borse, W. Choi, J. S. Lee, *Angew. Chem. Int. Ed.* **2005**, *44*, 4585.
[200] Z. Liu, Z.-G. Zhao, M. Miyauchi, *J. Phys. Chem. C* **2009**, *113*, 17132.

[201] J. Choi, S. Y. Ryu, W. Balcerski, T. K. Leeb, M. R. Hoffmann, *J. Mater. Chem.* **2008**, *18*, 2371.
[202] Y.-F. Lin, Y.-J. Hsu, *Appl. Catal. B* **2013**, *130–131*, 93.
[203] Z. Khan, M. Khannam, N. Vinothkumar, M. Deb, M. Qureshi, *J. Mater. Chem.* **2012**, *22*, 12090.
[204] C. Nasr, S. Hotchandani, W. Y. Kim, R. H. Schmehl, P. V. Kamat, *J. Phys. Chem. B* **1997**, *101*, 7480.
[205] D. Barpuzary, Z. Khan, N. Vinothkumar, M. De, M. Qureshi, *J. Phys. Chem. C* **2012**, *116*, 150.
[206] X. Wang, G. Liu, Z.-G. Chen, F. Li, L. Wang, G. Q. Lu, H.-M. Cheng, *Chem. Commun.* **2009**, 3452.
[207] P. Tongying, V. V. Plashnitsa, N. Petchsang, F. Vietmeyer, G. J. Ferraudi, G. Krylova, M. Kuno, *J. Phys. Chem. Lett.* **2012**, *3*, 3234.
[208] L. Huang, X. Wang, J. Yang, G. Liu, J. Han, C. Li, *J. Phys. Chem. C* **2013**, *117*, 11584.
[209] Y. Liu, Y.-X. Yu, W.-D. Zhang, *J. Phys. Chem. C* **2013**, *117*, 12949.
[210] L. L. Xu, J. G. Guan, W. D. Shi, *ChemCatChem* **2012**, *4*, 1353.
[211] T.-H. Yu, W.-Y. Cheng, K.-J. Chao, S.-Y. Lu, *Nanoscale* **2013**, *5*, 7356.
[212] F. A. Frame, F. E. Osterloh, *J. Phys. Chem. C*, **2010**, *114*, 10628
[213] Z. Zhang, P. Wang, *J. Mater. Chem.* **2012**, *22*, 2456.
[214] L. Yu, Y. Huang, G. Xiao, D. Li, *J. Mater. Chem. A* **2013**, *1*, 9637.
[215] J. Zhang, J. Yu, Y. Zhang, Q. Li, J. R. Gong, *Nano Lett.* **2011**, *11*, 4774.
[216] A. M. Schultz, P. A. Salvador, G, S. Rohrer, *Chem. Commun.* **2012**, *48*, 2012.
[217] Z. Zhang, G. Liu, Y. Mao, *Int. J. Hydrogen Energy* **2013**, *38*, 9349.
[218] Y. Hou, F. Zuo, A. Dagg, P. Feng, *Nano Lett.* **2012**, *12*, 6464.
[219] Y. Hou, F. Zuo, A. Dagg, P. Feng, *Angew. Chem. Int. Ed.* **2013**, *52*, 1248.
[220] C. Miao, S. Ji, G. Xu, G. Liu, L. Zhang, C. Ye, *ACS Appl. Mater. Interfaces* **2012**, *4*, 4428.
[221] K. J. McDonald, K.-S. Choi, *Chem. Mater.* **2011**, *23*, 4863.
[222] P. Dhanasekaran, H. G. Salunke, N. M. Gupta, *J. Phys. Chem. C* **2012**, *116*, 12156.
[223] Z. Liu, F. Chen, Y. Gao, Y. Liu, P. Fang, S. Wang, *J. Mater. Chem. A* **2013**, *1*, 7027.
[224] J. Shen, Y. Zhu, X. Yang, C. Li, *J. Mater. Chem.* **2012**, *22*, 13341.
[225] K. M. Parida, A. Nashim, S. K. Mahanta, *Dalton Trans.* **2011**, *40*, 12839.
[226] D. Wang, Z. Zou, J. Ye, *Chem. Mater.* **2005**, *17*, 3255.
[227] A. Nashim, S. Martha, K. M. Parida, *ChemCatChem* **2013**, *5*, 2352.
[228] J. Lv, T. Kako, Z. Zou, J. Ye, *Appl. Phys. Lett.* **2009**, *95*, 032107.
[229] C.M. Leroy, A. E. Maegli, K. Sivula, T. Hisatomi, N. Xanthopoulos, E. H. Otal, S. Yoon, A. Weidenkaff, R. Sanjinesd, M. Grätzel, *Chem. Commun.* **2012**, *48*, 820.
[230] S. Nazir, U. Schwingenschlögl, *Appl. Phys. Lett.* **2011**, *99*, 073102.
[231] J. Xing, Z. Shan, K. Li, J. Bian, X Lin, W. Wang, F. Huang, *J. Phys. Chem. Solids* **2008**, *69*, 23.
[232] M. Shahid, I. Shakir, S.-J. Yang, D. J. Kang, *Mater. Chem. Phys.* **2010**, *124*, 619.
[233] J. Zhang, J. H. Bang, C. Tang, P. V. Kamat, *ACS Nano* **2010**, *4*, 387.
[234] Y. Jia, S. Shen, D. Wang, X. Wang, J. Shi, F. Zhang, H. Han, C. Li, *J. Mater. Chem. A* **2013**, *1*, 7905.
[235] Z. Wang, J. Hou, S. Jiao, K. Huang, H. Zhu, *J. Mater. Chem.* **2012**, *22*, 21972.
[236] J. L. Gunjakar, T. W. Kim, H. N. Kim, I. Y. Kim, S.-J. Hwang, *J. Am. Chem. Soc.* **2011**, *133*, 14998.
[237] J. He, Z. Yan, J. Wang, J. Xie, L. Jiang, Y. Shi, F. Yuan, F. Yu, Y. Sun, *Chem. Commun.* **2013**, *49*, 6761.
[238] G.-H. He, C.-J. Liang, Y.-D. Ou, D.-N. Liu, Y.-P. Fang, Y.-H. Xu, *Mater. Res. Bull.* **2013**, *48*, 2244.
[239] M. Shi, X. Pan, W. Qiu, D. Zheng, M. Xu, H. Chen, *Int. J. Hydrogen Energy* **2011**, *36*, 15153.
[240] C. Ng, A. Iwase, Y. H. Ng, R. Amal, *J. Phys. Chem. Lett.* **2012**, *3*, 913.
[241] J. Cao, B. Luo, H. Lin, B. Xu, S. Chen, *Appl. Catal. B* **2012**, *111–112*, 288.
[242] K. Sivula, F. Le Formal, M. Grätzel, *Chem. Mater.* **2009**, *21*, 2862.
[243] S. K. Pilli, R. Janarthanan, T. G. Deutsch, T. E. Furtak, L. D. Brown, J. A. Turner, A. M. Herring, *Phys. Chem. Chem. Phys.* **2013**, *15*, 14723.
[244] S. Shenawi-Khalil, V. Uvarov, S. Fronton, I. Popov, Y. Sasson, *Appl. Catal. B* **2012**, *117–118*, 148.
[245] T. W. Kim, S.-J. Hwang, Y. Park, W. Choi, J.-H. Choy, *J. Phys. Chem. C* **2007**, *111*, 1658.
[246] A. Sheikh, A. Yengantiwar, M. Deo, S. Kelkar, S. Ogale, *Small* **2013**, *9*, 2091.
[247] K.-Z. Zhang, B.-Z. Lin, Y.-L. Chen, B.-H. Xu, X.-T. Pian, J.-D. Kuang, B. Li, *J. Colloid Interface Sci.* **2011**, *358*, 360.
[248] J. Jiang, X. Zhang, P. Sun, L. Zhang, *J. Phys. Chem. C* **2011**, *115*, 20555.
[249] G. K. Pradhan, S. Martha, K. M. Parida, *ACS Appl. Mater. Interfaces* **2012**, *4*, 707.
[250] Z. Wang, B. Huang, Y. Dai, X. Qin, X. Zhang, P. Wang, H. Liu, J. Yu, *J. Phys. Chem. C* **2009**, *113*, 4612.
[251] X. Wang, G. Liu, L. Wang, Z.-G. Chen, G. Q. (Max) Lu, H.-M. Cheng, *Adv. Energy Mater.* **2012**, *2*, 42.
[252] S. Cho, J.-W. Jang, J. S. Lee, K.-H. Lee, *Nanoscale* **2012**, *4*, 2066.
[253] F. Wen, X. Wang, L. Huang, G. Ma, J. Yang, C. Li, *ChemSusChem* **2012**, *5*, 849.
[254] B. Seger, A. B. Laursen, P. C. K. Vesborg, T. Pedersen, O. Hansen, S. Dahl, I. Chorkendorff, *Angew. Chem. Int. Ed.* **2012**, *51*, 9128.
[255] J. Liebig, *Ann. Pharm.* **1834**, *10*, 1.
[256] D. Mitoraj, H. Kisch, *Angew. Chem. Int. Ed.* **2008**, *47*, 9975.
[257] X. Wang, K. Maeda, A. Thomas, K. Takanabe, G. Xin, J. M. Carlsson, K. Domen, M. Antonietti, *Nat. Mater.* **2009**, *8*, 76.
[258] Y. Zheng, J. Liu, J. Liang, M. Jaroniec, S. Z. Qiao, *Energy Environ. Sci.* **2012**, *5*, 6717, and references within.
[259] F. Su, S. C. Mathew, G. Lipner, X. Fu, M. Antonietti, S. Blechert, X. Wang, *J. Am. Chem. Soc.* **2010**, *132*, 16299.
[260] X. Lu, Q. Wang, D. Cui, *J. Mater. Sci. Technol.* **2010**, *26*, 925.
[261] N. Yang, G. Li, W. Wang, X. Yang, W. F. Zhang, *J. Phys. Chem. Solids* **2011**, *72*, 1319.
[262] M. Bledowski, L. Wang, A. Ramakrishnan, O. V. Khavryuchenko, V. D. Khavryuchenko, P.C. Ricci, J. Strunk, T. Cremer, C. Kolbeck, R. Beranek, *Phys. Chem. Chem. Phys.* **2011**, *13*, 21511.
[263] B. Chai, T. Peng, J. Mao, K. Lia, L. Zan, *Phys. Chem. Chem. Phys.* **2012**, *14*, 16745.
[264] X. Zhou, B. Jin, L. Li, F. Peng, H. Wang, H. Yu, Y. Fang, *J. Mater. Chem.* **2012**, *22*, 17900.
[265] K. Kondo, N. Murakami, C. Ye, T. Tsubota, T. Ohno, *Appl. Catal. B* **2013**, *142–143*, 362.
[266] S. Kumar, T. Surendar, A. Baruah, V. Shanker, *J. Mater. Chem. A* **2013**, *1*, 5333.
[267] L. Ge, C. Han, J. Liu, *Appl. Catal. B* **2011**, *108–109*, 100.
[268] Y. Wang, X. Bai, C. Pan, J. Heb, Y. Zhu, *J. Mater. Chem.* **2012**, *22*, 11568.
[269] S. Zhang, Y. Yang, Y. Guo, W. Guo, M. Wang, Y. Guo, M. Huo, *J. Hazard. Mater.* **2013**, *261*, 235.
[270] J. Fu, Y. Tian, B. Chang, F. Xi, X. Dong, *J. Mater. Chem.* **2012**, *22*, 21159.
[271] L. Ye, J. Liu, Z. Jiang, T. Peng, L. Zan, *Appl. Catal. B* **2013**, *142–143*, 1.
[272] L. Ge, F. Zuo, J. Liu, Q. Ma, C. Wang, D. Sun, L. Bartels, P. Feng, *J. Phys. Chem. C* **2012**, *116*, 13708.
[273] J. Fu, B. Chang, Y. Tian, F. Xi, X. Dong, *J. Mater. Chem. A* **2013**, *1*, 3083.

[274] F. Yang, V. Kuznietsov, M. Lublow, C. Merschjann, A. Steigert, J. Klaer, A. Thomas, T. Schedel-Niedrig, *J. Mater. Chem. A* **2013**, *1*, 6407.
[275] S. Ye, L.-G. Qiu, Y.-P. Yuan, Y.-J. Zhu, J. Xia, J.-F. Zhu, *J. Mater. Chem. A*, **2013**, *1*, 3008.
[276] X. Zhou, B. Jin, R. Chen, F. Peng, Y. Fang, *Mater. Res. Bull.* **2013**, *48*, 1447.
[277] Q. Li, B. Yue, H. Iwai, T. Kako, J. Ye, *J. Phys. Chem. C* **2010**, *114*, 4100.
[278] L. Ge, C. Han, X. Xiao, L. Guo, *Int. J. Hydrogen Energy* **2013**, *38*, 6960.
[279] X. Wang, G. Chen, C. Zhou, Y. Yu, G. Wang, *Eur. J. Inorg. Chem.* **2012**, *2012*, 1742.
[280] X. Xu, G. Liu, C. Randorn, J. T. S. Irvine, *Int. J. Hydrogen Energy* **2011**, *36*, 13501.
[281] H. W. Kang, S. N. Lim, D. Song, S. B. Park, *Int. J. Hydrogen Energy* **2012**, *37*, 11602.
[282] S. C. Yan, S. B. Lv, Z. S. Li, Z. G. Zou, *Dalton Trans.* **2010**, *39*, 1488.
[283] Y. Zang, L. Li, Y. Zuo, H. Lin, G. Li, X. Guan, *RSC Adv.* **2013**, *3*, 13646.
[284] Y. Wang, R. Shi, J. Lin, Y. Zhu, *Energy Environ. Sci.* **2011**, *4*, 2922.
[285] L. Sun, X. Zhao, C.-J. Jia, Y. Zhou, X. Cheng, P. Li, L. Liu, W. Fan, *J. Mater. Chem.* **2012**, *22*, 23428.
[286] C. Pan, J. Xu, Y. Wang, D. Li, Y. Zhu, *Adv. Funct. Mater.* **2012**, *22*, 1518.
[287] Y. Hou, A. B. Laursen, J. Zhang, G. Zhang, Y. Zhu, X. Wang, S. Dahl, I. Chorkendorff, *Angew. Chem. Int. Ed.* **2013**, *52*, 3621.
[288] G. Liu, P. Niu, H.-M. Cheng, *Chem. Phys. Chem.* **2013**, *14*, 885.
[289] Y.-P. Yuan, S.-W. Cao, Y.-S. Liao, L.-S. Yin, C. Xue, *Appl. Catal. B* **2013**, *140–141*, 164.
[290] J. Zhang, M. Zhang, R.-Q. Sun, X. Wang, *Angew. Chem. Int. Ed.* **2012**, *51*, 10145.
[291] U. Stafford, K. A. Gray, P. V. Kamat, A. Varma, *Chem. Phys. Lett.* **1993**, *205*, 55.
[292] D. C. Hurum, A. G. Agrios, K. A. Gray, T. Rajh, M. C. Thurnauer, *J. Phys. Chem. B* **2003**, *107*, 4545.
[293] R. I. Bickley, T. Gonzalez-Carreno, J. S. Lees, L. Palmisano, R. J. D. Tilley, *J. Solid. State Chem.* **1991**, *92*, 178.
[294] T. Ohno, K. Sarukawa, K. Tokieda, M. Matsumura, *J. Catal.* **2001**, *203*, 82.
[295] T. Ohno, K. Tokieda, S. Higashida, M. Matsumura, *Appl. Catal. A* **2003**, *244*, 383.
[296] R. R. Bacsa, J. Kiwi, *Appl. Catal. B* **1998**, *16*, 19.
[297] J. Yu, J. C. Yu, W. Hoa, Z. Jiang, *New J. Chem.* **2002**, *26*, 607.
[298] B. Sun, P. G. Smirniotis, *Catal. Today* **2003**, *88*, 49.
[299] C. Wu, Y. Yue, X. Deng, W. Hua, Z. Gao, *Catal. Today* **2004**, *93–95*, 863.
[300] M. Yan, F. Chen, J. Zhang, *Chem. Lett.* **2004**, *33*, 1352.
[301] S. Bakardjieva, J. Subrt, V. Stengl, M. J. Dianez, M. J. Sayagues, *Appl. Catal. B* **2005**, *58*, 193.
[302] N. R. C. Fernandes Machado, V. S. Santana, *Catal. Today* **2005**, *107–108*, 595.
[303] M. Yan, F. Chen, J. Zhang, M. Anpo, *J. Phys. Chem. B* **2005**, *109*, 8673.
[304] D. Jiang, S. Zhang, H. Zhao, *Environ. Sci. Technol.* **2007**, *41*, 303.
[305] T. van der Meulen, A. Mattson, L. Österlund, *J. Catal.* **2007**, *251*, 131.
[306] A. Zachariah, K. V. Baiju, S. Shukla, K. S. Deepa, J. James, K. G. K. Warrier, *J. Phys. Chem. C* **2008**, *112*, 11345.
[307] J. Zhang, Q. Xu, Z. Feng, M. Li, C. Li, *Angew. Chem. Int. Ed.* **2008**, *47*, 1766.
[308] G. Li, S. Ciston, Z. V. Saponjic, L. Chen, N. M. Dimitrijevic, T. Rajh, K. A. Gray, *J. Catal.* **2008**, *253*, 105.
[309] J. Yu, G. Wang, *J. Phys. Chem. Solids* **2008**, *69*, 1147.
[310] Y.-C. Hsu, H.-C. Lin, C.-H. Chen, Y.-T. Liao, C.-M. Yang, *J. Solid State Chem.* **2010**, *183*, 1917.
[311] J. Yu, B. Wang, *Appl. Catal. B* **2010**, *94*, 295.
[312] Y. K. Kho, A. Iwase, W. Y. Teoh, L. Mädler, A. Kudo, R. Amal, *J. Phys. Chem. C* **2010**, *114*, 2821.
[313] V. Etacheri, M. K. Seery, S. J. Hinder, S. C. Pillai, *Chem. Mater.* **2010**, *22*, 3843
[314] R. G. Nair, S. Paul, S.K. Samdarshi, *Sol. Energy Mater. Sol. Cells* **2011**, *95*, 1901.
[315] T.-T. Duong, D.-J. Kim, C.-S. Kim, S.-G. Yoon, *J. Mater. Chem.* **2011**, *21*, 16473.
[316] T. A. Kandiel, R. Dillert, A. Feldhoff, D. W. Bahnemann, *J. Phys. Chem. C* **2010**, *114*, 4909.
[317] Y. Liu, Z. Wang, W. Wang, W. Huang, *J. Catal.* **2013**, DOI: 10.1016/j.jcat.2013.03.024.
[318] T. Alammar, H. Noei, Y. Wang, A.-V. Mudring, *Nanoscale* **2013**, *5*, 8045.
[319] R. Su, R. Bechstein, L. Sø, R. T. Vang, M. Sillassen, B. Esbjörnsson, A. Palmqvist, F. Besenbacher, *J. Phys. Chem. C* **2011**, *115*, 24287.
[320] Q. Sun, Y. Xu, *J. Phys. Chem. B* **2010**, *114*, 18911.
[321] B. Ohtani, O. O. Prieto-Mahaney, D. Li, R. Abe, *J. Photochem. Photobiol. A* **2010**, *216*, 179.
[322] L. Kavan, M. Grätzel, S. E. Gilbert, C. Klemenz, H. J. Scheel, *J. Am. Chem. Soc.* **1996**, *118*, 6716.
[323] T. Kawahara, Y. Konishi, H. Tada, N. Tohge, J. Nishii, S. Ito, *Angew. Chem. Int. Ed.* **2002**, *41*, 2811.
[324] T. Miyagi, M. Kamei, T. Mitsuhashi, T. Ishigaki, A. Yamazaki, *Chem. Phys. Lett.* **2004**, *390*, 399.
[325] H. Nakajima, T. Mori, Q. Shen, T. Toyoda, *Chem. Phys. Lett.* **2005**, *409*, 81.
[326] G. Xiong, R. Shao, T. C. Droubay, A. G. Joly, K. M. Beck, S. A. Chambers, W. P. Hess, *Adv. Funct. Mater.* **2007**, *17*, 2133.
[327] D. C. Hurum, A. G. Agrios, S. E. Crist, K. A. Gray, T. Rajh, M. C. Thurnauer, *J. Electron. Spectrosc.* **2006**, *150*, 155.
[328] P. Deák, B. Aradi, T. Frauenheim, *J. Phys. Chem. C* **2011**, *115*, 3443.
[329] J. T. Carneiro, T. J. Savenije, J. A. Moulijn, G. Mul, *J. Phys. Chem. C* **2011**, *115*, 2211.
[330] D. O. Scanlon, C. W. Dunnill, J. Buckeridge, S. A. Shevlin, A. J. Logsdail, S. M. Woodley, C. R. A. Catlow, M. J. Powell, R. G. Palgrave, I. P. Parkin, G. W. Watson, T. W. Keal, P. Sherwood, A. Walsh, A. A. Sokol, *Nat. Mater.* **2013**, *12*, 798.
[331] T. Ozawa, M. Iwasaki, H. Tada, T. Akita, K. Tanaka, S. Ito, *J. Colloid Int. Sci.* **2005**, *281*, 510.
[332] J. Yu, L. Zhang, B. Cheng, Y. Su, *J. Phys. Chem. C* **2007**, *111*, 10582.
[333] T. A. Kandiel, A. Feldhoff, L. Robben, R. Dillert, D. W. Bahnemann, *Chem. Mater.* **2010**, *22*, 2050.
[334] Q. Tay, X. Liu, Y. Tang, Z. Jiang, T. C. Sum, Z. Chen, *J. Phys. Chem. C* **2013**, *117*, 14973.
[335] T. A. Kandiel, L. Robben, A. Alkaima, D. Bahnemann, *Photochem. Photobiol. Sci.* **2013**, *12*, 602.
[336] H. Zhao, L. Liu, J. M. Andino, Y. Li, *J. Mater. Chem. A* **2013**, *1*, 8209.
[337] X. Wang, Q. Xu, M. Li, S. Shen, X. Wang, Y. Wang, Z. Feng, J. Shi, H. Han, C. Li, *Angew. Chem. Int. Ed.* **2012**, *51*, 13089.
[338] J. Hou, C. Yang, Z. Wang, W. Zhou, S. Jiao, H. Zhu, *Appl. Catal. B* **2013**, *142–143*, 504.
[339] Y. Sun, W. Wang, L. Zhang, Z. Zhang, *Chem. Eng. J.* **2012**, *211–212*, 161.
[340] M.-Y. Tsang, N. E. Pridmore, L. J. Gillie, Y.-H. Chou, R. Brydson, R. E. Douthwaite, *Adv. Mater.* **2012**, *24*, 3406.
[341] Z. Wang, J. Hou, C. Yang, S. Jiao, K. Huang, H. Zhu, *Energy Environ. Sci.* **2013**, *6*, 2134.
[342] Z. Chen, T. F. Jaramillo, T. G. Deutsch, A. Kleinman-Shwarsctein, A. J. Forman, N. Gaillard, R. Garland, K. Takanabe, C. Heske, M. Sunkara, E. W. McFarland, K. Domen, E. L. Miller, J. A. Turner, H. N. Dinh, *J. Mater. Res.* **2010**, *25*, 3.